

aval Research Laboratory

ashington, DC 20375-5000



NRL Report 9108

Aerosol Charge Distributions Produced By Radioactive Ionizers

W. A. HOPPEL AND G. M. FRICK

*Atmospheric Physics Branch
Space Science Division*

May 18, 1988

REPORT DOCUMENTATION PAGE				Form Approved OMB No. 0704-0188	
1a. REPORT SECURITY CLASSIFICATION UNCLASSIFIED			1b. RESTRICTIVE MARKINGS		
2a. SECURITY CLASSIFICATION AUTHORITY		3. DISTRIBUTION / AVAILABILITY OF REPORT			
2b. DECLASSIFICATION / DOWNGRADING SCHEDULE		Approved for public release; distribution unlimited.			
4. PERFORMING ORGANIZATION REPORT NUMBER(S) NRL Report 9108			5. MONITORING ORGANIZATION REPORT NUMBER(S)		
6a. NAME OF PERFORMING ORGANIZATION Naval Research Laboratory		6b. OFFICE SYMBOL (If applicable) Code 4110	7a. NAME OF MONITORING ORGANIZATION		
6c. ADDRESS (City, State, and ZIP Code) Washington, DC 20375-5000			7b. ADDRESS (City, State, and ZIP Code)		
8a. NAME OF FUNDING / SPONSORING ORGANIZATION Office of Naval Research		8b. OFFICE SYMBOL (If applicable)	9. PROCUREMENT INSTRUMENT IDENTIFICATION NUMBER		
8c. ADDRESS (City, State, and ZIP Code)			10. SOURCE OF FUNDING NUMBERS		
		PROGRAM ELEMENT NO. 61153N	PROJECT NO. RR033-02-42	TASK NO. 41-2101	WORK UNIT ACCESSION NO. DN480-215
11. TITLE (Include Security Classification) Aerosol Charge Distributions Produced by Radioactive Ionizers					
12. PERSONAL AUTHOR(S) Hoppel, W. A. and Frick, G. M.					
13a. TYPE OF REPORT		13b. TIME COVERED FROM _____ TO _____	14. DATE OF REPORT (Year, Month, Day) 18 May 1988		15. PAGE COUNT 39
16. SUPPLEMENTARY NOTATION					
17. COSATI CODES			18. SUBJECT TERMS (Continue on reverse if necessary and identify by block number)		
FIELD	GROUP	SUB-GROUP	Ionizers Singly charged particles Aerosols		
19. ABSTRACT (Continue on reverse if necessary and identify by block number)					
<p>This report is an analysis of the physical mechanisms that control the aerosol charge distribution established by radioactive neutralizers. Theoretical calculations and modeling is supplemented by experimental findings obtained with both commercially available ionizers and ionizers of our own design.</p>					
20. DISTRIBUTION / AVAILABILITY OF ABSTRACT <input checked="" type="checkbox"/> UNCLASSIFIED/UNLIMITED <input type="checkbox"/> SAME AS RPT. <input type="checkbox"/> DTIC USERS			21. ABSTRACT SECURITY CLASSIFICATION UNCLASSIFIED		
22a. NAME OF RESPONSIBLE INDIVIDUAL W. A. Hoppel			22b. TELEPHONE (Include Area Code) (202) 767-2362		22c. OFFICE SYMBOL Code 4110

CONTENTS

1.	INTRODUCTION	1
2.	BIPOLAR CHARGING IN AN UNBOUNDED REGION	2
	2.1 Symmetric Charging	3
	2.2 High Ionization Rate—Asymmetric Charging	4
	2.3 Low Ionization Rate or High Aerosol Concentration, $Z \gg n$	6
	2.4 Relaxation Time for Aerosol Charging	7
	2.5 Aerosol Charging After the Ionization Is Terminated	9
3.	ION CONCENTRATIONS AND AEROSOL CHARGING DURING FLOW THROUGH A CHANNEL CONTAINING AN IONIZER	9
	3.1 Relative Importance of Different Processes	11
	3.2 Comparison Between Experiments and Modeling Results	13
4.	SUMMARY STATEMENTS	14
5.	EXPERIMENTAL RESULTS	16
	5.1 Evaluation of NRL Ionizers	16
	5.2 Evaluation of Commercially Available Ionizers	16
6.	DESIGN OF AN IONIZER THAT PRODUCES A NEAR-SYMMETRIC EQUILIBRIUM CHARGE DISTRIBUTION	18
7.	CONCLUSIONS	20
8.	REFERENCES	20
	APPENDIX A — Ammonium Sulfate Aerosol Generation by Gas Phase Reaction	22
	APPENDIX B — Measurements of Ion Current vs Collector Voltage	26
	APPENDIX C — Time-Dependent Charging Calculations	29
	APPENDIX D — Ion-Aerosol Attachment Coefficient Calculation	32

AEROSOL CHARGE DISTRIBUTIONS PRODUCED BY RADIOACTIVE IONIZERS

1. INTRODUCTION

The mechanical generation of particles often produces an aerosol that is highly charged. The charge can be neutralized by passing the aerosol through an irradiated region where the production of ions creates a zone of high electrical conductivity. In this region the aerosol charge is conducted from the particles to the walls of the neutralizer. The charge distribution on an aerosol that has undergone a neutralization process is often assumed to be described by Boltzmann statistics with no net charge (equal numbers of positively and negatively charged particles). While this description of charge neutralization is adequate for many processes in which the terminal charge distribution is of little consequence, it is not adequate for certain applications. The differential mobility analyzer (DMA) size spectrometer, in particular, requires accurate knowledge of the charge distribution in order to invert the mobility distribution measured with the DMA to a size distribution.

Undoubtedly the most widely used theory to predict the charge distribution is Boltzmann statistics (Keefe, Nolan, and Rich, 1959). This theory does not allow for the differences in positive and negative ions and thus predicts symmetric charging; it also does not give the time required to achieve equilibrium. Diffusion charging theories allow for differences in the diffusion and mobility coefficients of the positive and negative ions and predict that charging in a balanced bipolar ion environment will produce a nonsymmetric aerosol charge. (For a review of bipolar charging theories, see Hoppel and Frick, 1986.) Since the charging depends on the ionic environment, an important first step is to understand the processes that occur in the ionizer. This study was motivated by confusing experimental results obtained when we attempted to test the validity of different charging theories by measuring the ratio of positively to negatively charged particles exiting neutralizers. It soon became apparent that the measured charge ratio was as much a function of the ionizer design as it was of the charging theory. This led us to study the factors that determine the ion concentrations in an ionizer. Much of our original confusion stemmed from our ignorance of what was actually occurring in and downstream of the ionized region.

This report is a study of the physical mechanisms that control the aerosol charge distribution established by radioactive neutralizers. The computations are of two types: (a) modeling the ion environment as the air moves over and downwind of a region of high ionization, and (b) calculating the aerosol charge distribution in ion environments with various polar ion ratios. Measurements were made of (a) the polar ion concentrations downwind of radioactive sources and (b) the degree of asymmetric charging produced by several ionizers, including a prototype neutralizer that produces a nearly symmetrical equilibrium charge distribution by adjusting the ratio of the polar ion concentrations to compensate for the differences in the ion properties.

2. BIPOLAR CHARGING IN AN UNBOUNDED REGION

The statistical charge state of a monodisperse aerosol is determined by the following system of balance equations (see, for example, Hoppel and Frick, 1986).

$$\frac{dn_1}{dt} = q - \alpha n_1 n_2 - n_1 \sum_{k=0}^{p-1} \beta_{11}^{(k)} N_1^{(k)} - n_1 \sum_{k=1}^p \beta_{12}^{(k)} N_2^{(k)}, \quad (1)$$

$$\frac{dn_2}{dt} = q - \alpha n_1 n_2 - n_2 \sum_{k=0}^{p-1} \beta_{22}^{(k)} N_2^{(k)} - n_2 \sum_{k=1}^p \beta_{21}^{(k)} N_1^{(k)}, \quad (2)$$

$$\frac{dN_0}{dt} = n_1 \beta_{12}^{(1)} N_2^{(1)} + n_2 \beta_{21}^{(1)} N_1^{(1)} - n_1 \beta_{10}^{(0)} N_0 - n_2 \beta_{20}^{(0)} N_0, \quad (3)$$

$$\frac{dN_1^{(k)}}{dt} = n_1 \beta_{11}^{(k-1)} N_1^{(k-1)} - n_1 \beta_{11}^{(k)} N_1^{(k)} + n_2 \beta_{21}^{(k+1)} N_1^{(k+1)} - n_2 \beta_{21}^{(k)} N_1^{(k)}, \quad (4)$$

$$\frac{dN_2^{(k)}}{dt} = n_2 \beta_{22}^{(k-1)} N_2^{(k-1)} - n_2 \beta_{22}^{(k)} N_2^{(k)} + n_1 \beta_{12}^{(k+1)} N_2^{(k+1)} - n_1 \beta_{12}^{(k)} N_2^{(k)}, \quad (5)$$

$$Z = N_0 + \sum_{k=1}^p N_1^{(k)} + \sum_{k=1}^p N_2^{(k)}, \quad (6)$$

where n_1 and n_2 are the positive and negative ion concentrations respectively, $\beta_{ij}^{(k)}$ are the attachment coefficients between an ion of polarity i and a particle with k charges of polarity j , $N_j^{(k)}$ is the concentration of positive or negative particles with k charges, Z is the total concentration that is held constant with time, q is the ionization rate, and α is the recombination coefficient. There is one more equation than the number of variables. In the limit as the system approaches steady state, Eq. (3) is not independent of Eqs. (4) and (5); we therefore chose to eliminate Eq. (3). For symmetric charging, the concentrations of positive and negative ions are the same, as are the numbers of positively and negatively charged particles; thus charge conservation is inherent. For the nonsymmetric case, these equations need to be supplemented with the charge conservation equation:

$$n_1 - n_2 + \sum_{k=1}^p k N_1^{(k)} - \sum_{k=1}^p k N_2^{(k)} = \frac{\rho_0}{e}, \quad (7)$$

where ρ_0 is the initial space charge (obtained from the initial conditions).

It is often convenient to simplify the equations by assuming fixed ion ratios and steady state conditions, for which case the aerosol balance equations decouple from the ion balance equations. The principle of detailed balancing (Gunn, 1955) requires that

$$n_i \beta_{ii}^{(k-1)} N_i^{(k-1)} = n_j \beta_{ji}^{(k)} N_i^{(k)}. \quad (8)$$

In Eqs. (4) and (5) this requires that the first and fourth terms and the second and third terms balance separately. (The necessity of this requirement at steady state can be demonstrated by terminating the

above system of equations at some finite value of k .) Solving for the number of particles with k charges in terms of uncharged particles gives

$$\frac{N_i^{(k)}}{N_0} = \left(\frac{n_i}{n_j} \right)^k \prod_{m=1}^k \frac{\beta_{ii}^{(m-1)}}{\beta_{ji}^{(m)}}. \quad (9)$$

The charge distribution $f_i^{(k)}$ describes the fraction of particles carrying k charges of sign i .

$$f_i^{(k)}(r) = \frac{N_i^{(k)}(r)}{Z} = \frac{N_i^{(k)}/N_0}{Z/N_0}, \quad (10)$$

where the numerator is Eq. (9) and the denominator is obtained from Eqs. (6) and (9):

$$\frac{Z}{N_0} = 1 + \sum_{k=1}^p \left[\left(\frac{n_i}{n_j} \right)^k \prod_{m=1}^k \frac{\beta_{ii}^{(m-1)}}{\beta_{ji}^{(m)}} + \left(\frac{n_j}{n_i} \right)^k \prod_{m=1}^k \frac{\beta_{jj}^{(m-1)}}{\beta_{ij}^{(m)}} \right]. \quad (11)$$

These equations do not include any diffusive or electrically driven fluxes of ions or aerosols to the walls of the container. Because of the higher diffusion coefficient of ions, their diffusive loss to the walls is much greater than for the aerosol. The loss of ions to the walls is considered in Section 3.

The most widely used diffusion theory for determining the ion-aerosol attachment coefficients is that of Fuchs (1964). Fuchs' theory is reviewed, and a theory that includes three-body trapping is presented in a paper by Hoppel and Frick (1986), which provides attachment coefficients for ions of mobilities of 1.2 and 1.35 cm² V⁻¹ s⁻¹ (atmospheric ions at standard temperature and pressure (STP), (Mohnen, 1977)). The use of these values of mobility together with the Nolan value of 1.4 × 10⁻⁶ cm³ s⁻¹ were motivated by our interest in the interaction of ions and aerosols in the atmosphere (Hoppel, 1985). For higher ion concentrations (shorter ion lifetimes) as exist downwind of the ionizer, more appropriate values of positive and negative ion mobilities would be 1.3 and 1.8 cm² V⁻¹ s⁻¹ respectively, at STP and an ion-ion recombination coefficient of 1.6 × 10⁻⁶ cm³ s⁻¹. The resulting negative to positive mobility ratio of about 1.4 is in good agreement with the measurements downwind of the ionizers reported in Appendix B. The recombination coefficients have been recalculated with these values of mobilities and are given in Appendix D, together with a discussion of the method of calculations. In this report we use the values of β given in Appendix D.

2.1 Symmetric Charging

Symmetric charging is an ideal process for which the positive and negative ions are assumed to be identical except for their polarity, thus $\beta_{ij} = \beta_{ji}$, $\beta_{ii} = \beta_{jj}$, and $n_1 = n_2$. Consequently, the charge distribution is symmetric and Eqs. (9) and (10) become

$$\frac{N_i^{(k)}}{Z} = \frac{\prod_{m=1}^k \beta_{ii}^{(m-1)}/\beta_{ij}^{(m)}}{1 + 2 \sum_{k=1}^p \prod_{m=1}^k \beta_{ii}^{(m-1)}/\beta_{ji}^{(m)}}. \quad (12)$$

Figure 1 shows the numerical solution (discussed later) to Eqs. (5) through (11) for the case when $q = 10^4$ cm⁻³ s⁻¹. The calculations are for 0.05- μ m radius particles, using values of β for ions of

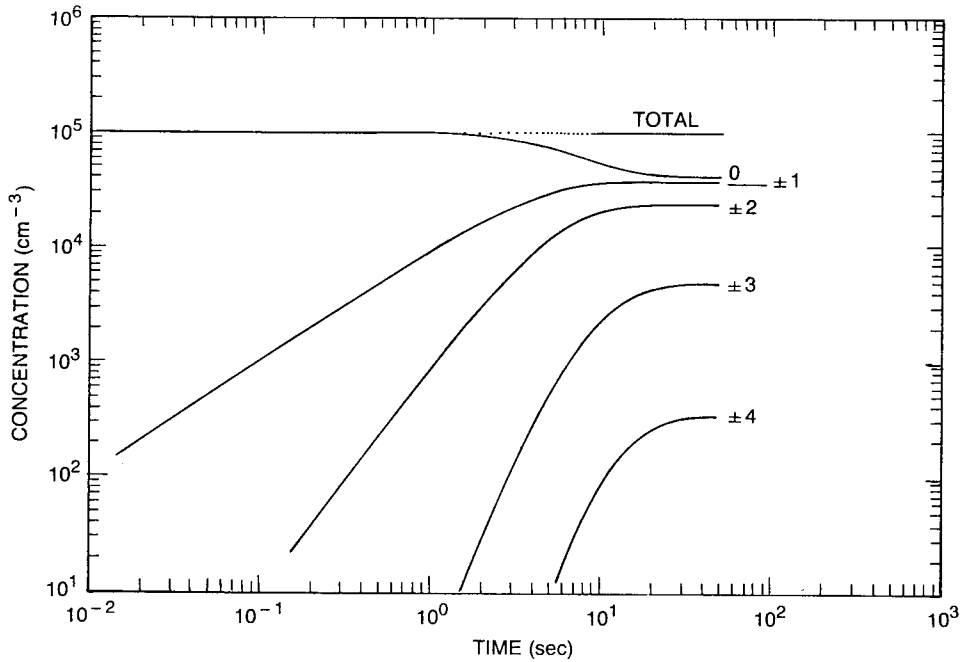


Fig. 1 — Time-dependent symmetric charging of an initially uncharged monodisperse aerosol ($r = 0.05 \mu\text{m}$) by ions of mobility $\mu = 1.3 \text{ cm}^2 \text{ V}^{-1} \text{ s}^{-1}$

mobility $1.3 \text{ cm}^2 \text{ V}^{-1} \text{ s}^{-1}$. If the calculations are repeated, using values of β for $1.8 \text{ cm}^2 \text{ V}^{-1} \text{ s}^{-1}$ for both positive and negative ions, the equilibrium charge distribution is nearly identical but is achieved somewhat sooner. The equilibrium distribution is shown in Fig. 2 as a function of size. The equilibrium charge distribution is nearly independent of the ionic properties in the symmetric case. It is interesting to note that the Boltzmann theory predicts that the charge distribution (shown by the dashed line in Fig. 2) is totally independent of the ionic properties. The fact that the charge distribution is nearly independent of ionic properties for symmetric charging will later be used as an argument for the design of a neutralizer that produces a near-symmetric aerosol charge distribution.

2.2 High Ionization Rate—Asymmetric Charging

In a region of very high ionization (and aerosol concentrations limited so that $n \gg Z$), the ion densities are determined by the balance between the rates of ionization and recombination. These are symmetric processes and produce an environment where the polar ion concentrations are equal. In the high-ionization limit, any ionic imbalance caused by the unequal attachment of positive and negative ions to the aerosol has negligible effect on the ion concentrations. In this case Eqs. (9), (10), and (11) together with the assumption of equal ion densities can be used to calculate the asymmetric charge distribution. Assuming values of β corresponding to positive ions of mobility 1.3 and values of β for negative ions of mobility of 1.8 (given in Appendix D), we obtain Fig. 3. This charge distribution is obviously much different from that shown in Fig. 2 and illustrates that, for real situations where aerosols are neutralized in a region of high ionization, we should expect the charge distribution to be asymmetric.

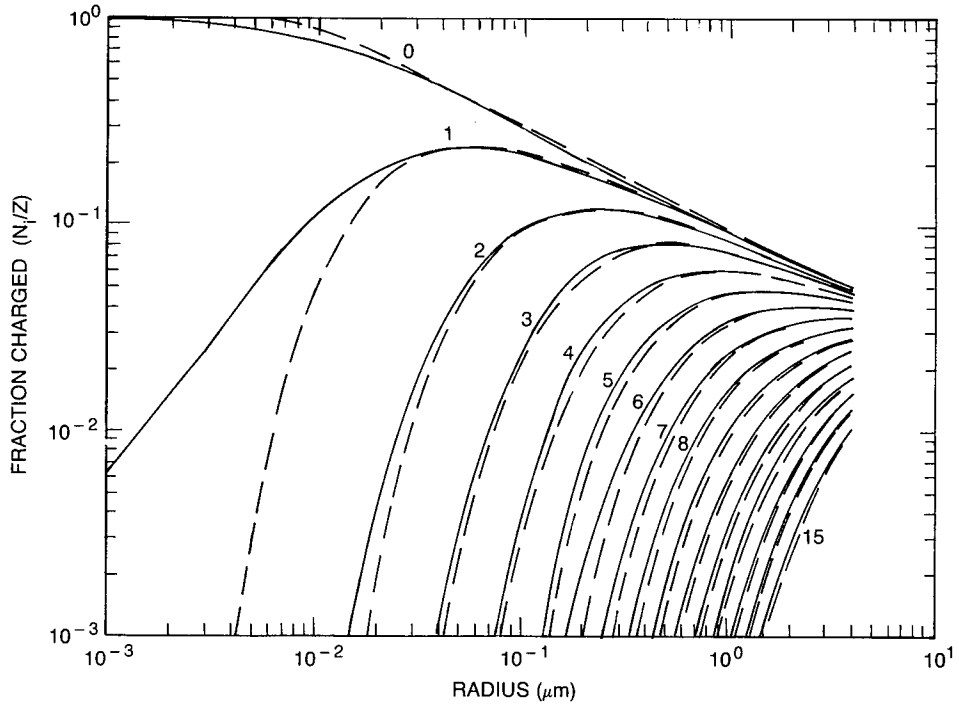


Fig. 2 — Symmetric equilibrium charge distribution of Hoppel and Frick (1986).
The Boltzmann charge distribution is given by the dashed line.

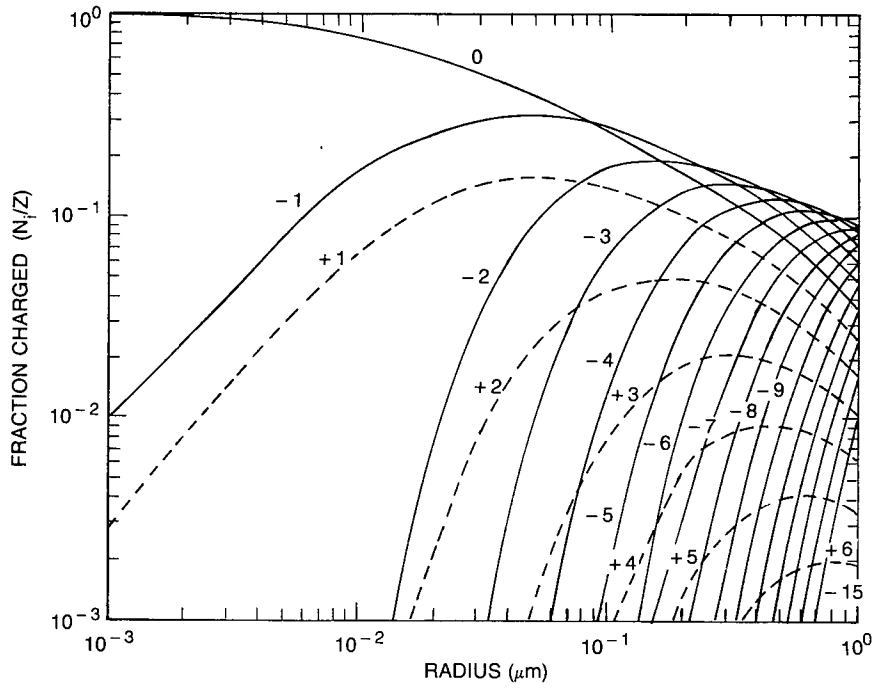


Fig. 3 — Asymmetric charge distribution as a function of radius for
 $n_- = n_+$, $\mu_+ = 1.3 \text{ cm}^2 \text{ V}^{-1} \text{ s}^{-1}$, and $\mu_- = 1.8 \text{ cm}^2 \text{ V}^{-1} \text{ s}^{-1}$

Figure 4 displays the charge distribution for particles of radius 0.01, 0.05, and 0.2 μm as a function of the number of elementary charges. The dashed line gives the charge distribution derived by Gunn (1955) for the case when the radius is larger than 0.05 μm . The Gunn expression is

$$\frac{N^{(k)}}{Z} = \frac{e}{(2\pi rKT)^{1/2}} \exp \left\{ \frac{-[k - (rKT/e^2)\ln(\mu_1 n_1/\mu_2 n_2)]^2}{2rKT} \right\}, \quad (13)$$

where K is Boltzmann's constant, T is the absolute temperature, and μ_1 and μ_2 are the ionic mobilities. Gunn's expression was developed for particles of radii greater than 0.05 μm ; this creates an inconsistency regarding the sum of charged and uncharged particles for smaller sizes, as is evident for the 0.01- μm size. Gunn's expression is similar to the Boltzmann charge distribution except that it is offset from $k = 0$ by a factor related to the ratio of the polar conductivities. For the case shown (high ionization) we have assumed that the ion concentrations are equal, and therefore the offset is due only to the difference in the polar ion mobilities.

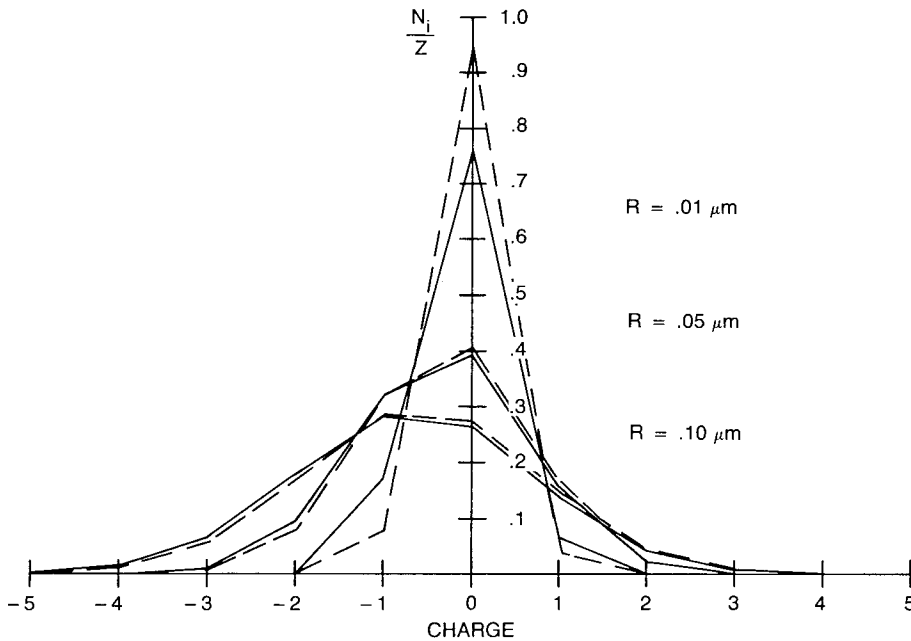


Fig. 4 — Fraction of particles carrying k elementary charges for particles of 0.01, 0.05, and 0.1 μm radius calculated for positive and negative ion mobilities of 1.3 and 1.8 $\text{cm}^2 \text{V}^{-1} \text{s}^{-1}$ respectively. The dashed line is from Eq. (13).

Once the sample leaves the region of high ionization, the ion concentration decays very rapidly, and it may be impossible to maintain conditions such that the ion concentration is determined only by symmetric processes (e.g., recombination). An imbalance in the polar ion concentrations develops when the ion loss to aerosols and/or the walls is comparable to loss by ion-ion recombination.

2.3 Low Ionization Rate or High Aerosol Concentrations, $Z \gg n$

For a low ionization rate and/or high aerosol concentration, the loss of ions to the aerosol particles is the dominant sink for ions (the particles act as recombination centers for the ions). If there is initially no net space charge, then charge conservation requires that the concentrations of positively and negatively charged particles be equal. Production of this symmetric aerosol charge requires the

positive to negative ion ratio to be greater than unity (Eq. (9)). This imbalance of charge on the less numerous ions must, of course, be balanced by a small difference in the polar charge ratio carried by particles (the ratio will still be near unity). An important example of the low ionization case is a polluted atmosphere for which the concentration of ions due to natural radioactivity is much less than the concentration of aerosols. In a neutralizer, charge equilibrium must be achieved rapidly, which requires the high ion concentrations provided by high ionization rates. The convergence of the charged particle ratio to unity as the ionization is decreased is shown in Hoppel and Frick (1986). This calculation has been replotted in Fig. 5 (using the values of β given in Appendix D) in terms of the ratio of ion loss by recombination to the loss by attachment of aerosols.

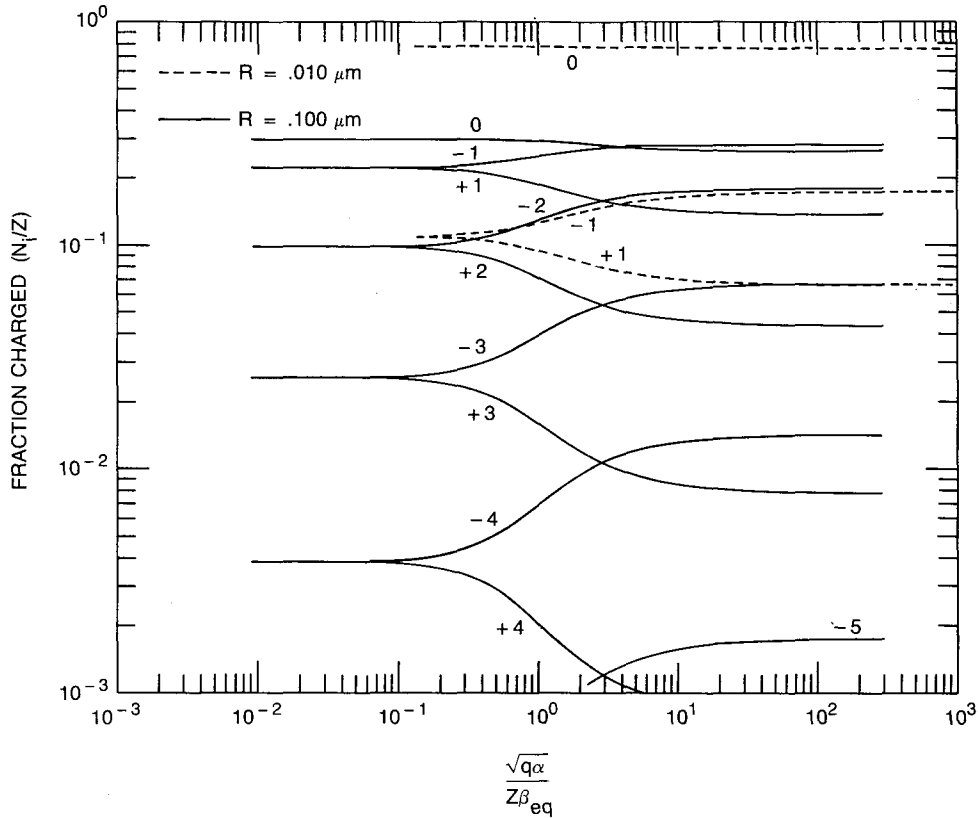


Fig. 5 — Imbalance in positive and negative particles as a function of the dimensionless parameter $(q\alpha)^{1/2}/\beta Z$ for particles of 0.01 and 0.1 μm radius

2.4 Relaxation Time for Aerosol Charging

The time-dependent charging and/or discharging of aerosols has been modeled by applying a Runge-Kutta method to solve Eqs. (1) through (7), for which the values of β were taken from Appendix D. Solutions for particles of radius 0.01 and 0.1 μm are shown in Figs. 6 and 7 and illustrate the approach to equilibrium as an initially uncharged aerosol is exposed to a region where the ionization rate is 10^5 ion pair cm^{-3} and the recombination coefficient is taken to be 1.6×10^{-6} $\text{cm}^3 \text{s}^{-1}$. The numbers on the curves correspond to the number of elementary charges on the particles. The total particle concentration in each case is 10^4 . For 0.01- μm particles, there are no multiply charged particles. If we were to assume that the ionization rate is sufficiently high that ion

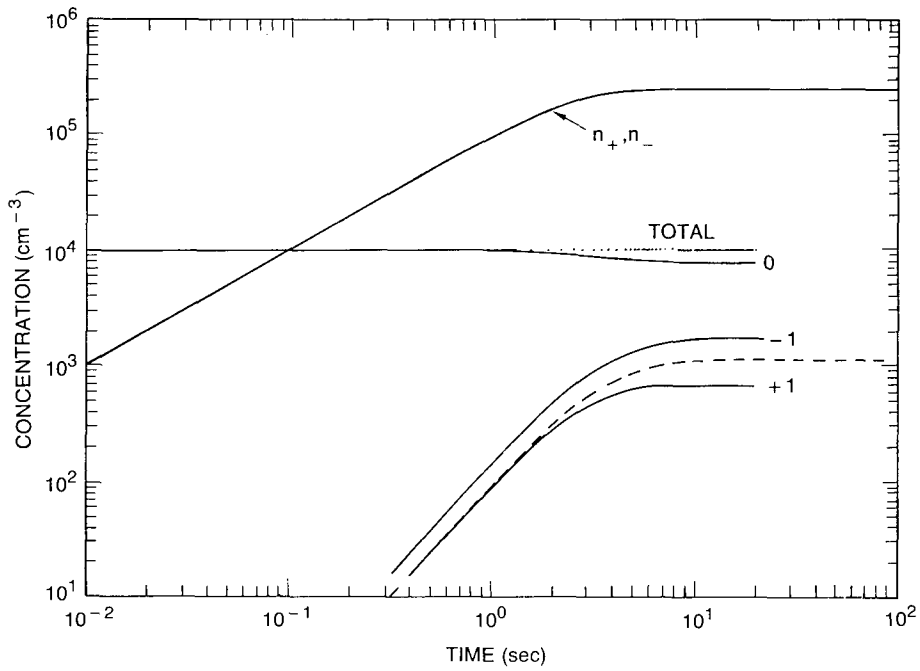


Fig. 6 — Asymmetric charging of particles of radius 0.01 μm in a region where the ionization rate is 10⁵ ion pairs cm⁻³ s⁻¹

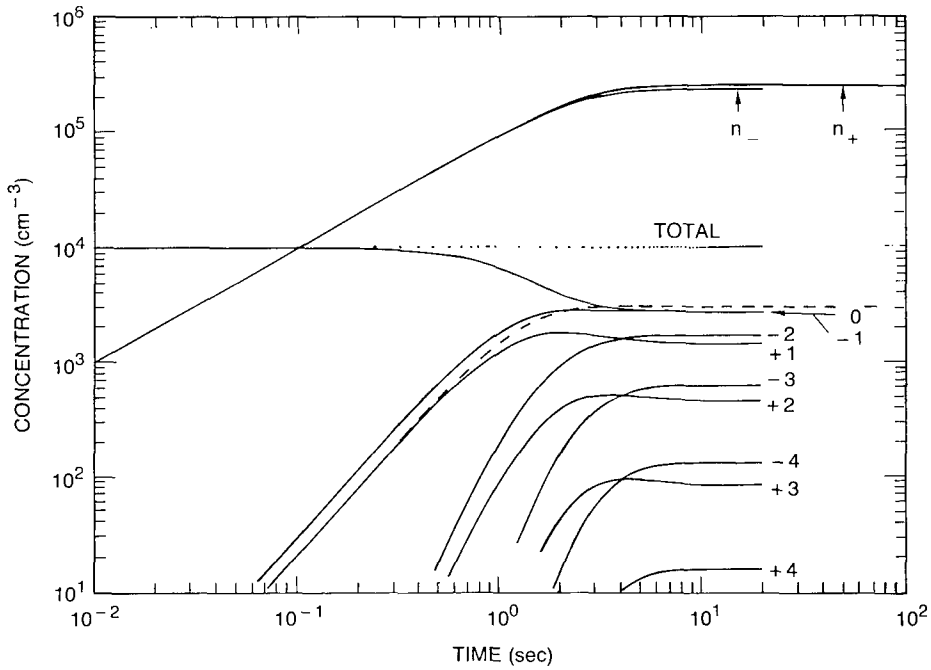


Fig. 7 — Asymmetric charging of particles of radius 0.1 μm in a region where the ionization rate is 10⁵ ion pairs cm⁻³ s⁻¹

recombination dominates ion loss to the particles and the charging is symmetric, then the ion equations decouple from the aerosol equations and an analytic solution is possible. The solutions for the ion concentrations and fraction of singly charged particles are:

$$\text{and} \quad n_+ = n_- = (q\alpha)^{1/2} \tanh [(\alpha q)^{1/2} t] \quad (14)$$

$$\frac{N_1}{Z} = \frac{\beta_0}{2\beta_0 + \beta_1} \left\{ 1 - \left[\frac{2}{\cosh (2t\sqrt{\alpha q}) + 1} \right]^{\frac{2\beta_0 + \beta_1}{2\alpha}} \right\}. \quad (15)$$

These analytic solutions are shown by dashed lines in Figs. 6 and 7 and give nearly the same result as the rigorous solution for the 0.01- μm size. For the 0.1- μm particles (Fig. 7), multiply charged particles are important. Since a $k + 1$ charged particle is derived from a particle with k charges, it appears at a later time. The dashed lines are again obtained from Eqs. (14) and (15) where the values of β used were the coefficients for single charging and discharging events; multiply charged particles are neglected. Equations (14) and (15) are given here so that estimates of the time required for equilibrium over a radioactive source can be obtained without resorting to the numerical solution of the complete set of equations.

Appendix C presents further graphical solutions of aerosol charging and discharging under various conditions.

2.5 Aerosol Charging After the Ionization Is Terminated

In the event that the ionization source is abruptly removed after charge equilibrium is achieved, then the particles will age in a region of rapidly decaying ion concentrations. When the positive and negative ions have identical properties, the charge on the aerosols is symmetric and remains symmetric in the region of decaying ion concentrations because the polar ion ratio remains at unity. However, if for some reason there is a slight imbalance in the number of positive and negative ions, then conservation of charge requires that there be an ever-increasing ion ratio as the ions decay. In this case the aerosol charge distribution changes as a result of the changing ion ratio, and equilibrium will not exist. The initial ion imbalance may be caused by more rapid diffusion of one ion species to the walls or by some more exotic mechanism such as the expulsion of secondary electrons during radioactive decay. Figure 8 illustrates how the changing ion ratio during decay would affect the aerosol charge distribution if the initial ion ratio were 0.98. In the realistic case of ions with unequal diffusion coefficients, there will always be unequal wall losses that will be magnified in the ionic ratio downwind of the ionizing source, where the ion concentrations are decaying because of recombination. This indicates that the equilibrium charge established in the ionizer will be modified after the aerosol has been removed from the source region. Since in most ionizers there will be a region of decaying ion concentrations downwind of the radioactive source, either in the ionizer itself or in the plumbing, the ability of an ionizer to produce an equilibrium charge distribution on an aerosol is brought to question.

3. ION CONCENTRATIONS AND AEROSOL CHARGING DURING FLOW THROUGH A CHANNEL CONTAINING AN IONIZER

There are always ion losses to the walls and the plumbing between the ionization source and the measuring device. To explore the possibility of modification of the aerosol charge distribution

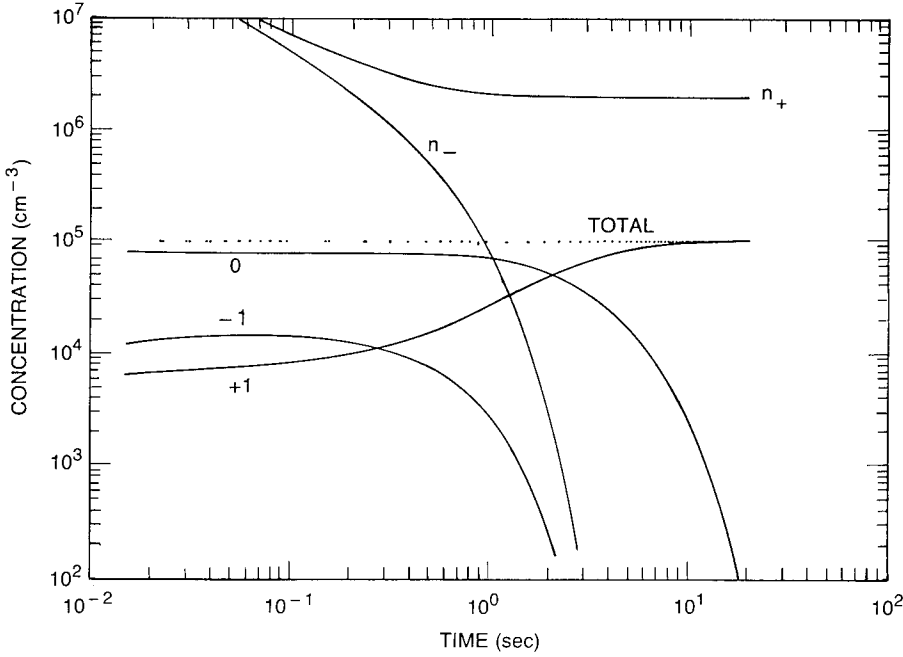


Fig. 8 — The increase in the ratio of the polar ion densities caused by an initial ion imbalance (2%) and its effect on the charge distribution of $0.01 \mu\text{m}$ radius particles

downwind of the ionization region, we have modeled the ion concentrations in a channel. The equations that govern the ion concentrations are:

$$\nabla \cdot J_1 = q - \alpha n_1 n_2, \quad (16)$$

$$\nabla \cdot J_2 = q - \alpha n_1 n_2, \quad (17)$$

and

$$\nabla \cdot E = \frac{e}{\epsilon}(n_1 - n_2), \quad (18)$$

and the ion fluxes are

$$J_{1,2} = \pm \mu_{1,2} E n_{1,2} + v n_{1,2} - D_{1,2} n_{1,2}, \quad (19)$$

where $D_{1,2}$ are the diffusion coefficients, E is the electric field resulting from any ionic space charge, e is the elementary charge, ϵ is the permittivity of air, and v is the flow velocity.

These equations include the following ionic effects: diffusion, electrical conduction to the walls, formation by volume ionization, and recombination. Diffusion and conduction parallel to the flow are assumed to be negligible compared to the perpendicular components, and the flow is assumed to have a parabolic profile. Also, ion-aerosol interactions are assumed to be unimportant in establishing the ion concentrations; an assumption that is only valid in a region where the ion concentrations are much larger than the aerosol concentrations.

3.1 Relative Importance of Different Processes

For illustrative purposes we have modeled the ion concentrations in a 2-cm-wide channel. The air flows over a radioactive source where it reaches an equilibrium ion concentration of 1×10^5 . Figure 9(a) shows the ion profiles at various distances downstream of the source for a parabolic flow profile with mean velocity of 6 cm/s. The solid line is for positive ions, and the dashed line is for negative ions (of mobilities 1.3 and $1.8 \text{ cm}^2 \text{ V}^{-1} \text{ s}^{-1}$), respectively. To understand the relative importance of the various physical processes, we compare modeled results for which a specific process has been disabled. Figure 9(a) shows the complete solution of Eqs. (16) through (19) for the ion profiles. The difference in the positive and negative profiles is due to the more rapid diffusion of negative ions to the walls.

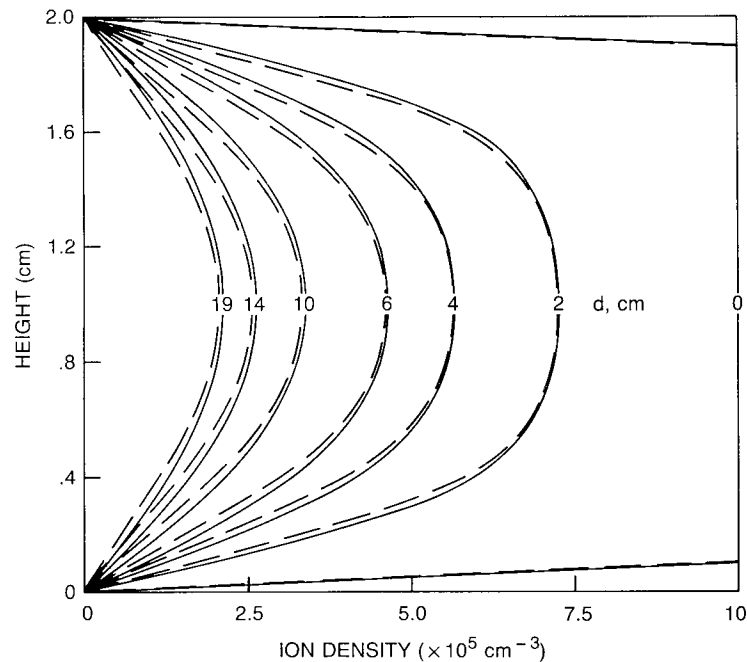


Fig. 9(a) — Complete solution for the evolution of the ion profiles in a 2-cm channel downwind of a bipolar ion source. Solid (dashed) lines are for positive (negative) ions.

Figure 9(b) shows that if ion recombination is omitted ($\alpha = 0$), the ion concentration decay is greatly slowed as the air flows down the tube. Since recombination is proportional to the product of the ion concentrations, recombination is the dominant loss mechanism at high ion concentrations. The profile shown in Figure 9(b) is largely the result of ionic diffusion to the walls. However, the electric field caused by the ionic space charge is also important in that it attracts negative ions from the walls and repels positive ions outward toward the walls. This limits the degree of ionic imbalance that can develop because of diffusion.

If diffusion to the walls is turned off, as illustrated by Fig. 9(c), the concentrations of positive and negative ions remain equal and there is no electric field to influence ion migration. The concentration profile develops because of the parabolic velocity profile; the air near the walls flows more slowly and the ions have more time to recombine. (If plug flow is assumed, then the concentration profile remains constant with height.)

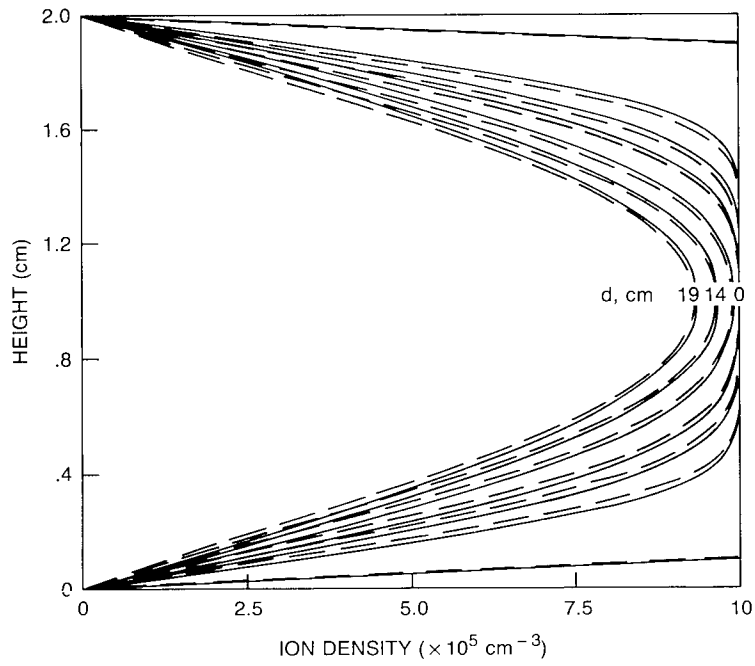


Fig. 9(b) — Change in solution (a) obtained when recombination is eliminated ($\alpha = 0$)

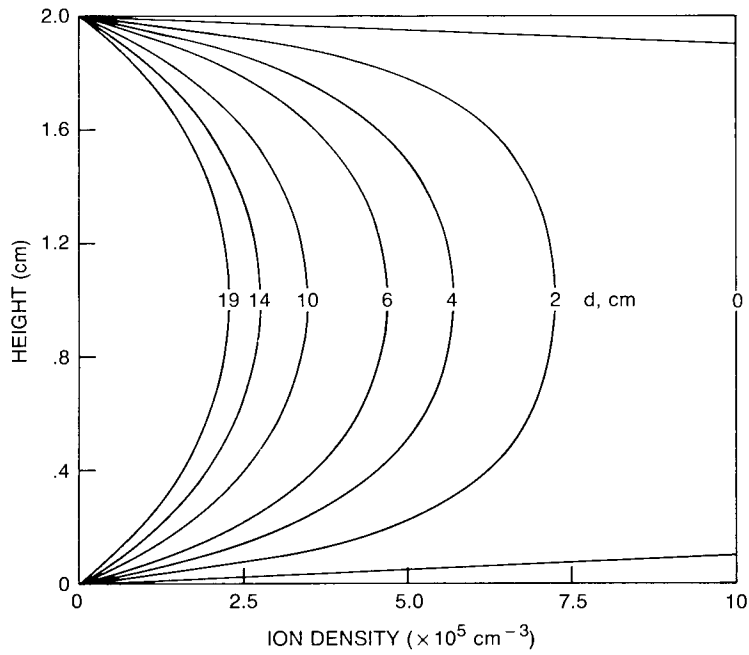


Fig. 9(c) — Change in solution (a) obtained by eliminating diffusion to the walls ($D_{+,-} = 0$)

Figure 9(d) shows that if electrical conduction is turned off by setting the ionic mobilities to zero, diffusion of negative ions to the walls exceeds that of the positive ions, producing a larger polar ion ratio (n_+/n_-) than would otherwise occur. This effect may appear to be a small contribution to the overall ion concentration, but its effect on the ion ratio is quite significant. In the case shown the predominance of positive ions has increased from 8% to 17% (profile average). As shown earlier, the ratio of the polar ion densities is important in determining the ratios of positively to negatively charged particles. Since the electric field is the integral of the space charge, the effect of the electric field is strongly dependent on the size of the neutralizer.

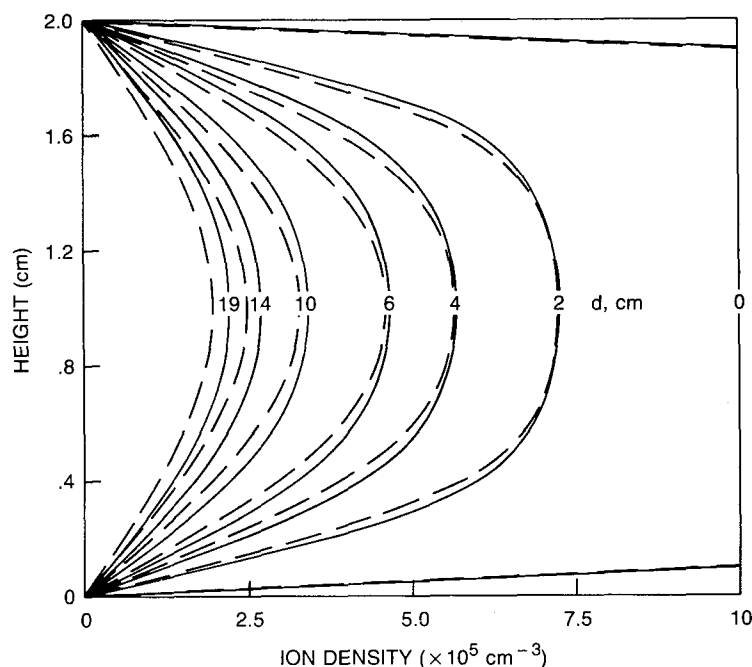


Fig. 9(d) — Change in solution (a) obtained by elimination of the mobilities of the ions in the electric field ($\mu_{+,-} = 0$)

3.2 Comparison Between Experiments and Modeling Results

Polar ion concentrations were measured for several distances downwind of a radioactive source ($5.3 \mu\text{Ci Am-241}$) within a rectangular ($1.9 \times 4.5 \text{ cm}$) tube. Ion concentrations were calculated from the expression:

$$n = \frac{i}{e\Phi}, \quad (20)$$

where i is the ion current, e is the electron charge, and Φ is the volumetric flow rate. This equation assumes that the voltage on the collector is large enough to collect all the ions, and therefore the measured concentrations represent the mean ion concentrations.

Figure 10 illustrates an experiment in which the radioactive source was positioned distances of 6, 12, and 18 cm from the shield wires. Shorter distances were not used because a series of I-V curves taken during a preliminary portion of this experiment revealed that current saturation was difficult to achieve at less than 6 cm (see Appendix B). Ion concentrations at the 6-cm location were used as an initial condition in the model, and an initial concentration profile was adopted to simulate the

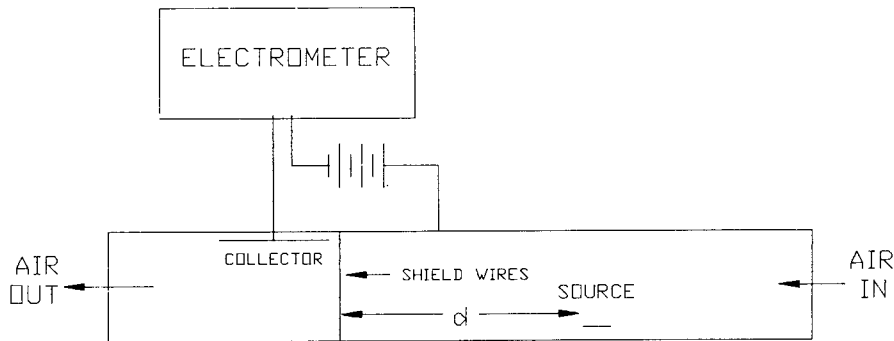


Fig. 10 — Experimental arrangement for measurement of ion concentrations downwind of a radioactive source

first 6 cm of travel. Figure 11 shows the computed concentrations of positive and negative ions 12 and 18 cm downwind of the source (the upper set of dashed lines), compared with the experimental data (the upper solid lines). Closer agreement could be obtained by adjusting the values used for recombination and mobility; however, since the model assumes parallel plates, whereas the experimental setup has side walls, precise agreement was not expected. A second comparison was performed in which the 6 cm immediately in front of the shield wires was spanned by a set of five parallel plates (each $4.0 \times 6.0 \times 0.05$ cm), spaced 0.3 cm apart; the source was located 6 cm upwind of this "diffusion cell" (12 cm from the shield wires). For this case, the measured concentration of the positive and negative ions is indicated by the lower solid lines of Fig. 11, and the computed concentrations are indicated by the lower set of dashed lines. In addition to the large diffusive losses expected in the diffusion cell, there is an increase in the polar ion ratio. This is because the smaller channels of the diffusion cell reduce the electric field caused by the ionic space charge, therefore a larger polar ion ratio can develop.

4. SUMMARY STATEMENTS

The following statements based on the preceding two sections summarize the mechanisms that are important in understanding the operation and design of radioactive neutralizers.

1. In a region of high volume ionization, the polar ion concentrations will be nearly equal.
2. When the ion concentrations are equal, there will be pronounced asymmetric charging owing to the difference in the positive and negative ion diffusivities (mobilities).
3. In the region of decaying ion concentrations downwind of a source, the polar ion ratio will be changing and no true equilibrium charge distribution can be maintained. In an ionizer this is due primarily to the unequal diffusion of positive and negative ions to the walls. However, even in the absence of walls, the charge distribution will change as the system evolves from an ion-dominated regime to an aerosol-dominated one, as is shown in Fig. 5.
4. Since the diffusion coefficients of positive and negative ions are unequal, large ratios of ion densities can be obtained in a diffusion-dominated region downwind of the region of high ionization. The magnitude of the polar ion imbalance will be limited by the ionic space charge as expressed by the next statement.
5. The effect of the electric field created by an imbalance in the polar ion concentrations limits the ionic imbalance that can be established by the unequal rates of diffusion of positive and negative ions to the walls. Since the electric field is proportional to the charge enclosed within the

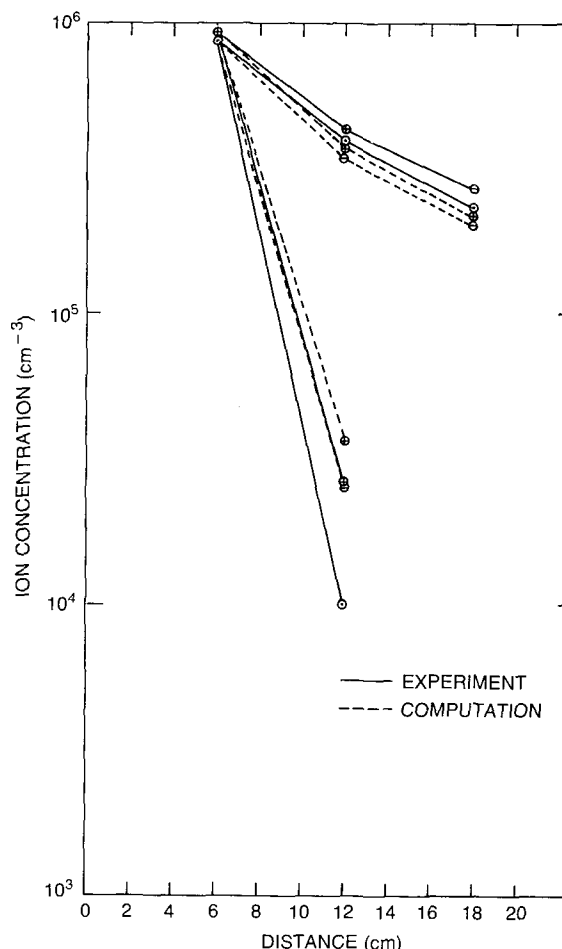


Fig. 11 — Computed and measured ion concentrations at distances of 12 and 18 cm downwind of the source. The upper set of lines pertains to the rectangular channel; the lower set of lines pertains to the diffusion cell with 0.3-cm plate spacing.

volume (Gauss' Law), the limiting effect of the field on the ion ratio is strongly dependent on the size of the neutralizer.

6. A symmetric charge distribution on an aerosol does not imply that the aerosol is in charge equilibrium. By using a diffusion-dominated region downwind of an ionizer, it is possible at some point to balance the faster diffusion of negative ions to the particles by a predominance of positive ions and obtain an aerosol with zero net charge. However, this is a transient state, not an equilibrium one, and should not necessarily agree with the predictions of an equilibrium theory of charging.
7. If the aerosol concentration is much greater than the ion concentration (low ionization rate) and if the net charge on the system is zero, then conservation of charge requires a symmetric charge on the aerosol. This case is usually of little importance in aerosol charging because the time for charging at low ionization rates is extremely long. However, this same effect can play a significant role downwind of the source in a long ionizer with larger cross section. The larger cross section prevents a large ion imbalance (statement 5), and the longer residence time allows the ion concentrations to decay to levels smaller than the aerosol concentrations. Since the negative

ions attach more readily to the particles, the positive to negative ion ratio increases and the ratio of charged particles approaches unity as required by conservation of charge (assuming the concentrations of ions are negligible compared to aerosols). Examples of this are discussed in Section 5.1 and in Appendix C.

5. EXPERIMENTAL RESULTS

5.1 Evaluation of NRL Ionizers

A pair of our early ionizers consist of sections of rectangular waveguide tubing (aluminum) with internal dimensions of 1.9×4.5 cm, lengths of 12.5 and 30 cm, with an Am-241 foil source (256 μCi), affixed approximately 2 cm from the inlet of each. The ends are sealed by plates fitted with tubing adapters. We use our ionizers in conjunction with a differential mobility analyzer (DMA) that has a sample flow rate of 50 cc/s, so the residence time of aerosols in the ionizers is roughly 2 and 5 s, respectively. An initially perplexing result was that the shorter ionizer consistently produced a ratio of negative to positive particles of about 1.3, whereas the longer ionizer produced ratios in the range of 1.8 to 2.1 (see Fig. 12), this was the opposite of what we had expected. Our initial prediction was that in the longer ionizer the ions would age and the ratio of mobilities would decrease as observed in laboratory experiments, thus producing a more balanced charge. However, our modeling results show that the shorter ionizer has sufficient numbers of ions exiting to substantially alter the aerosol charge distribution after the aerosol has left the ionizer. The small diameter of the tube downstream of the ionizer reduces the electric field due to the ionic imbalance and allows the negative ions to diffuse to walls, relatively unimpeded by the predominance of positive ions. In contrast, the longer ionizer has a substantially greater residence time downwind of the source, allowing the ion concentrations to decay to a much lower level before exiting. The electric field due to the ionic space charge prevents a large imbalance in the polar ion ratio while in the ionizer channel, and the concentrations of the exiting ions are now too low to substantially modify the aerosol charge distribution in the neutralizer.

An inverse relation between aerosol concentration and the ratio of negative to positive particles was also observed when the 30-cm-long ionizer was used. This is an example of the situation discussed in Section 2 and Statement 7 of Section 4, where the particles become the dominant sink for the ions. Figure 13 is a plot of the charged particle ratio vs the concentration of negative particles within a single channel of the DMA. For the specific aerosol used during this experiment (gas phase nucleation of sulfuric acid and ammonia as described in Appendix A), the value of 1000 particles/cc within the considered interval corresponds to a size distribution (similar to that presented in Fig. A3) that contains on the order of 20,000 particles/cc. The decrease of aerosol charge ratio to values less than 1.5 required total aerosol concentrations greater than 100,000/cc.

5.2 Evaluation of Commercially Available Ionizers

The negative to positive ratio of singly charged particles exiting two ionizers manufactured by Thermo Systems Inc. (TSI) and one ionizer produced by the University of Minnesota for the National Bureau of Standards (NBS) were measured as a function of particle radius by using the aerosol generation technique described in Appendix A and the differential mobility analyzer system depicted in Fig. A1. The dominance of singly charged particles was ensured by the steep slope of the size distribution as shown in Figs. A2 and A3. The ionizers tested were TSI models 3012 and 3077, and the ionizer loaned to us by NBS (which bore no identification). The behavior of the TSI model 3054 was also investigated, as will be described later. All of these ionizers use stainless steel encapsulated Kr-85 (beta) sources ranging from 2 to 10 millicuries (mCi). The TSI model 3012 is fitted with screens interior to both the inlet and outlet, a feature not present on the other ionizers. The results of these

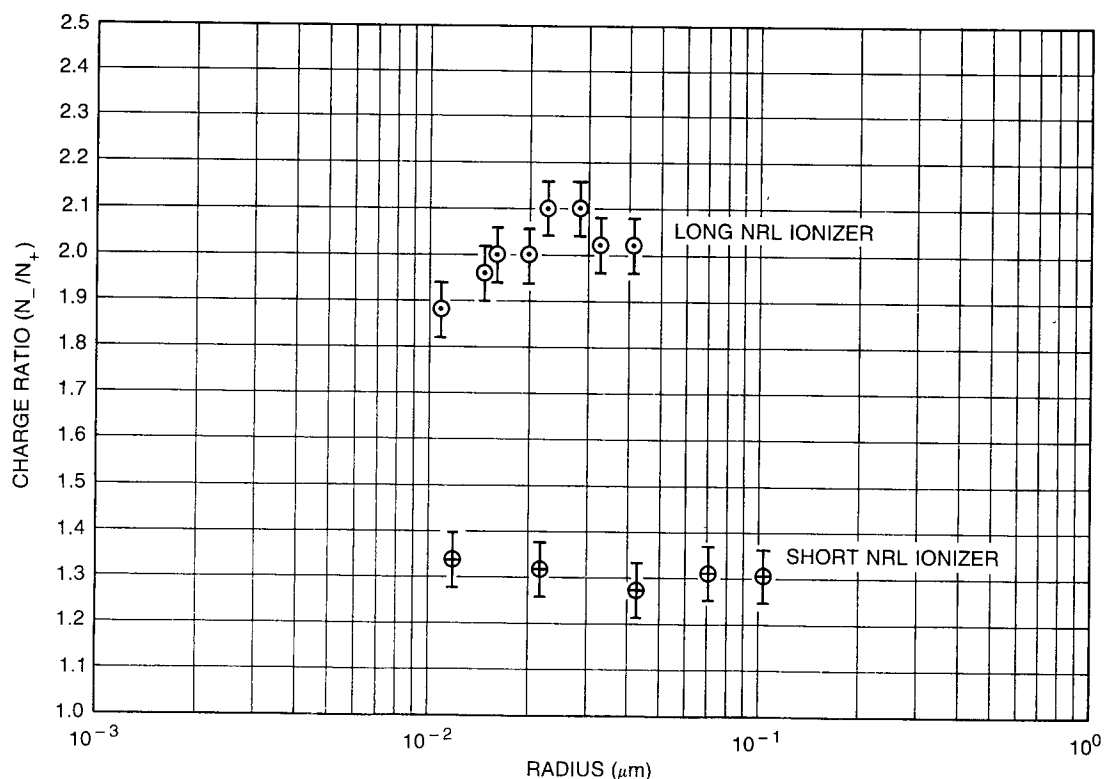


Fig. 12 — Evaluation of the particle charge ratio produced by two early NRL ionizers with different residence times

tests are presented in Fig. 14, which shows that none of these ionizers produced a truly symmetric charge distribution. A flow rate of 50 cc/s was used throughout the experiment, except for the few points noted. The physically smallest neutralizer, TSI model 3077, provided the charge distribution that was closest to symmetric from this group of ionizers. The significantly lower particle charge ratio (N_-/N_+) obtained with the TSI 3077 is attributed to the small-diameter tubing provided for inlet and outlet connections. These metal tubes, designed to reduce radiation leakage, are rather long and extend into the active region of the ionizer, so that the tube samples high ion concentrations that decay during passage through the tube. The diffusional loss of ions within the small-diameter tube results in an abundance of positive ions that alter the aerosol charge distribution obtained over the source (as in the case of the short NRL ionizer). As stated earlier, this is not an equilibrium process and the results will depend upon the flow rate and aerosol size distribution. In an effort to verify this effect, the particle charge ratio was determined for a TSI model 3054 neutralizer fitted with either a 7.0 or 3.5 mm ID metal tube 32 cm in length, at the exit. Comparisons were made between cases for which the metal tubes were inserted into the ionized region vs those for which the tube inlet coincided with the normal ionizer outlet. The particle charge ratio was reduced when the tube was inserted into the ionized region for both sizes of tube, from 1.65 to 1.44 for the larger diameter tube, and from 1.50 to 1.23 for the smaller diameter tube. As expected, the smaller diameter tube permits diffusion to establish a larger ion ratio before it is limited by the electric field (and before the ion concentrations are diminished by recombination). The fact that the size of the tube connected to the ionizer outlet affected the particle charge ratio indicates that sufficient ions exit the ionizer to alter the charge distribution while traversing downwind plumbing.

We emphasize that except for the TSI model 3077, these ionizers are designed to reduce the net charge of highly charged aerosols; however this does not guarantee zero net charge or charge equilibrium.

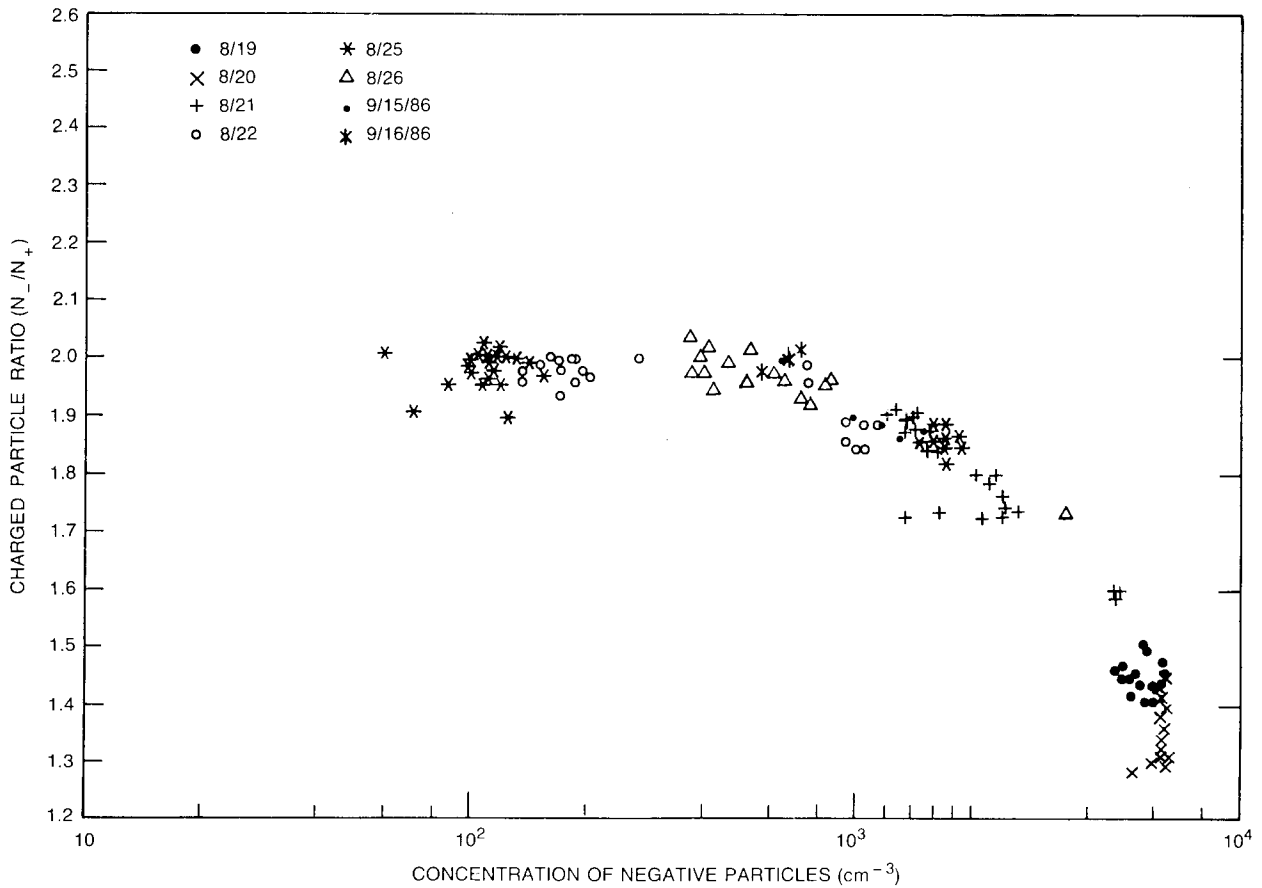


Fig. 13 — Plot of the ratio of negatively to positively charged particles ($0.015 < r < 0.022 \mu\text{m}$) vs concentration of negatively charged particles of the same radius. (The total concentration of particles is approximately 20 times the abscissa value.)

6. DESIGN OF AN IONIZER THAT PRODUCES A NEAR-SYMMETRIC EQUILIBRIUM CHARGE DISTRIBUTION

We previously stated that if positive and negative ions have different mobilities, there can be no equilibrium downwind of the ion source. This implies that removal of the ions immediately downwind of the source is necessary to eliminate the wall losses that alter the polar ion ratio. A neutralizer must also provide sufficient residence time for the aerosol within the ionized region to establish equilibrium. Symmetry of the charge distribution requires that the ratio of positive to negative ion concentrations compensate for the inequality in attachment coefficients of positive and negative ions. This may be accomplished by incorporating diffusion surfaces within the ionized region for the removal of more negative than positive ions; these surfaces can also serve to reduce the electric field associated with ion imbalance. The ion concentrations must be low enough so that ion diffusion losses are comparable to the losses due to recombination; yet the ion concentrations must also be substantially greater than the aerosol concentrations, or the aerosol charge distribution will be concentration dependent. To obtain the desired trade-off between the residence time required for aerosol charge equilibrium and the diffusive loss of aerosols to the walls, it is necessary to tailor the ionizer to a specific airflow and maximum aerosol load. In certain instances it may be advantageous to bring the aerosol close to charge equilibrium with a front-end ionizer prior to the final charge neutralization.

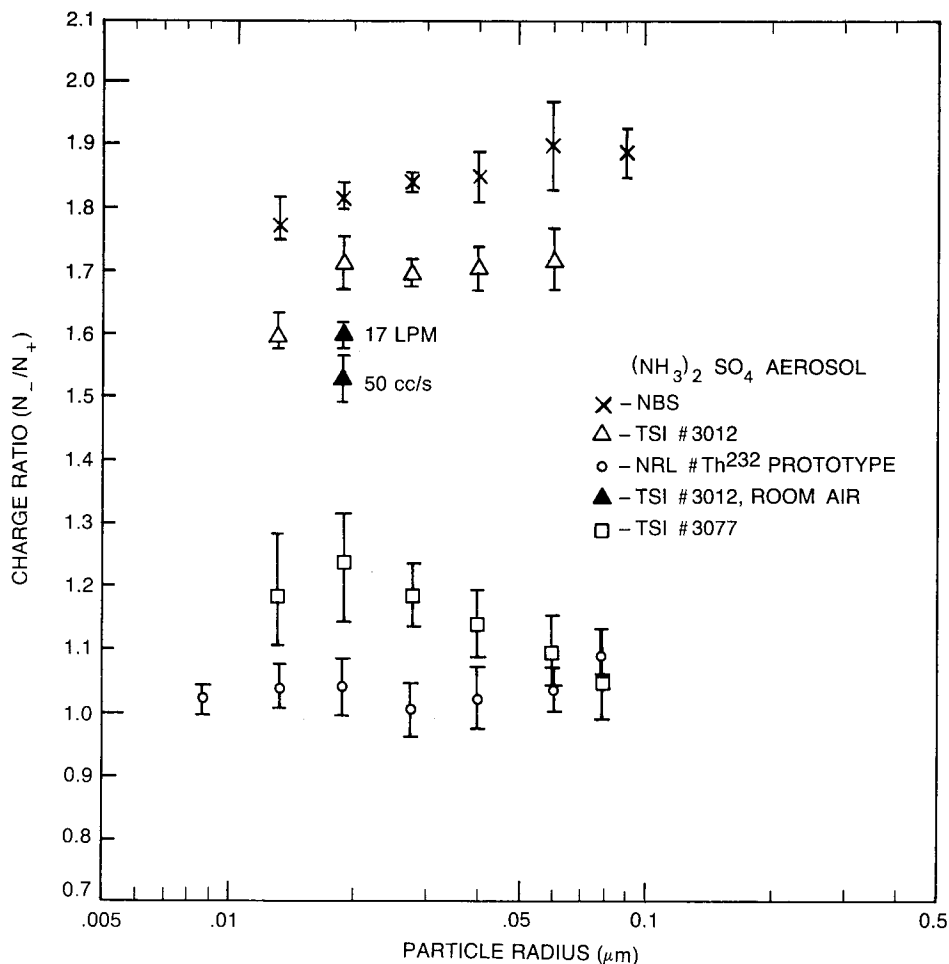


Fig. 14 — The ratio of negatively to positively charged particles obtained with four different ionizers

An ionizer based on the above requirements has been constructed (see Fig. 15), using a Th-232 sheet 4.0 cm wide and 18 cm long (total activity of 3.7 μCi) in conjunction with 10 diffusion plates that are perpendicular to the active sheet. This assembly is inserted into a rectangular section of tubing (1.9×4.5 cm cross section mentioned earlier), and ion removal is accomplished by a 4×3 cm plate immediately downwind of the source to which +20 V is applied. As shown in Fig. 14, this NRL prototype ionizer produced the most symmetric charge distribution of the ionizers tested. Estimates of the polar ion concentrations in the ionized region as determined from measurements immediately downwind of the ionizer indicated positive (negative) ion concentrations of 40,000 (21,000) per cc. Consideration of the aerosol flow rate, ionizer geometry, and ion mobility dictate the optimum voltage and/or length of the ion collection plate in order to minimize particle loss. The minimum residence time within the ionizer for establishment of aerosol charge equilibrium was estimated by using the aerosol charging model discussed in Section 2. The diffusion surface area was determined by trial and error measurements of the charged particle ratio. The loss of particles larger than 0.01 μm in this ionizer due to diffusion is not severe; both measurements and calculations indicate that the loss of 0.01 μm radius particles to be less than 5% at the prescribed flow rate of $50 \text{ cm}^3 \text{ s}^{-1}$.

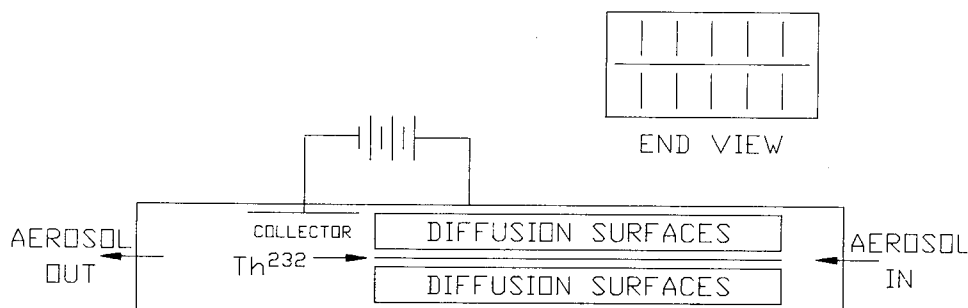


Fig. 15 — A prototype ionizer that produces a near symmetric aerosol charge distribution

7. CONCLUSIONS

The charge distributions of aerosols exiting radioactive neutralizers are the result of a complex relationship between the parameters of the neutralizer and the aerosol charging mechanism. In most (if not all) of the present ionizers, the charge distribution will be changing downwind of the source region and no truly equilibrium distribution can be maintained. The culprit is the changing polar ion ratio produced by the combination of ionic recombination and the more rapid diffusion of negative ions to the walls. The space charge electric field plays an important role in limiting the degree of ionic imbalance that will develop through unequal diffusion of positive and negative ions to the walls. This effect is strongly influenced by the size of the ionizer.

A number of studies (Hussin et al. (1983), Porstendorfer et al. (1984), Adachi et al. (1985), Kousaka et al. (1985)) have been initiated to test various charging theories. Each of these studies has relied on an ionizer to bring the aerosol to "charge equilibrium." This study suggests that these results may not be a valid test of the theory, since the measured charge distribution is most likely not only determined by the parameters of the theory but also by the particular ionizer, downwind plumb-ing geometry, and flow rate.

The results and understanding of the ionizer/neutralizer provided by this study will hopefully make it possible to develop a new family of neutralizers that produce a well-defined aerosol charge distribution. One such attempt has been reported in this report.

8. REFERENCES

- Adachi, M., Kousaka, Y., and Okuyama, K. (1985), "Unipolar and Bipolar Diffusion Charging of Ultrafine Aerosol Particles," *J. Aerosol Sci.* **16**, 109-123.
- Cabane, M., Krien, P., Madelaine, G., and Bricard, J. (1975), "Mobility Spectra of Ions Created in Gases Under Atmospheric Pressure," *J. Colloid Interface Sci.* **57**, 289-300.
- Fuchs, N.A. (1963), "On the Stationary Charge Distribution on Aerosol Particles in a Bipolar Ionic Atmosphere," *Geofis. Pura. Appl.* **56**, 185-193.
- Fuchs, N.A. (1964), "On the Steady-State Distribution of the Charges of Aerosol Particles in a Bipolarly Ionized Atmosphere," Series **4**, 579-586.
- Gunn, R. (1955), "The Statistical Electrification of Aerosols by Ionic Diffusion," *J. Colloid Sci.* **10**, 107.

- Hoppel, W.A. (1985), "Ion-Aerosol Attachment Coefficients, Ion Depletion, and the Charge Distribution on Aerosols," *J. Geophys. Res.* **90**, 5917-5923.
- Hoppel, W.A. and Frick, G.M. (1986), "Ion-Aerosol Attachment Coefficients and the Steady-State Charge Distribution on Aerosols in a Bipolar Ion Environment," *Aerosol Sci. Tech.* **5**, 1-21.
- Huertas, M.L. and Fontan, J. (1975), "Evolution Times of Tropospheric Positive Ions," *Atmos. Environ.* **9**, 1018-1026.
- Huertas, M.L., Fontan, J., and Gonzalez, J. (1978), "Evolution Times of Tropospheric Negative Ions," *Atmos. Environ.* **12**, 2351-2362.
- Hussin, A., Scheibel, H.G., Becker, K. H., and Porstendörfer, J. (1983), "Bipolar Diffusion Charging of Aerosol Particles — I. Experimental Results Within the Diameter Range 4-30 nm," *J. Aerosol Sci.* **14**, 671-677.
- Keefe, D., Nolan, P.J., and Rich, T.A. (1959), "Charge Equilibrium in Aerosols According to the Boltzmann Law," *Proc. R. Irish Acad.* **60A**, 27-44.
- Kousaka, Y., Okuyama, K., and Adachi, M. (1985), "Determination of Particle Size Distribution of Ultra-Fine Aerosol Using a Differential Mobility Analyzer," *Aerosol Sci. Tech.* **4**, 209-225.
- Meyerott, R.E., Reagan, J.B., and Joiner, R.G. (1980), "The Mobility and Concentration of Ions and the Ionic Conductivity in the Lower Stratosphere," *J. Geophys. Res.* **85**, 1273-1278.
- Mohnen, V.A. (1977), *Electrical Processes in Atmosphere*, H. Dolezalek and R. Reiter, eds. (Steinkopff Verlag, Darmstadt), pp 1-17.
- Nolan, P.J. (1943), "The Recombination Law for Weak Ionization," *Proc. Royal Irish Acad.* **49**, 67-90.
- Perkins, M.D. and Eisele, F.L. (1984), "First Mass Spectrometric Measurements of Atmospheric Ions at Ground Level," *J. Geophys Res.* **87**, 9649-9657.
- Porstendörfer, J., Hussin, A., Scheibel, H.G., and Becker, K.H. (1984), "Bipolar Diffusion Charging of Aerosol Particles — II. Influence of the Concentration Ratio of Positive and Negative Ions on the Charge Distribution," *J. Aerosol Sci.* **15**, 47-56.
- Wiendensohler, A., Lütke-meier, E., Feldpausch, M., and Helsper, C. (1986), "Investigation of the Bipolar Charge Distribution at Various Gas Conditions," *J. Aerosol Sci.* **17**, 413-426.

Appendix A

AMMONIUM SULFATE AEROSOL GENERATION BY GAS PHASE REACTION

A reproducible and stable source of aerosol particles in the 0.01 to 0.1 μm size range has been generated by the following technique. Figure A1 illustrates the aerosol generation and measurement arrangement. A stream of charcoal and absolute filtered room air is divided into three streams: acid, base, and dilution flows. The acid flow (typically 1 cc/s) is introduced at one end of a 5-cm-ID glass tube containing a 97% H_2SO_4 solution that has a surface area approximately 80 cm long and 4 cm wide. The acid is contained behind a glass dam at the downwind end of the surface. Air flowing over the acid contains very low concentrations of sulfuric acid vapor. The base flow (also typically 1 cc/s) is passed over the surface of a 0.05% solution NH_4OH contained in a 1-liter flask and exits from the top. The air containing NH_3 is combined with the air containing acid vapor immediately downwind of the dam. Aerosol formation by binary homogeneous nucleation is almost immediate. The flows are allowed to mix for the remaining length of the glass tube (40 cm) and then combined with the dilution flow (typically 48 cc/s) and used for the experiment. The use of a large volume holding chamber is not recommended (unless adequate mixing is available), for it was found that the aerosol concentrations were much more stable without it. Examples of aerosol size distributions are presented in Figs. A2 and A3 for which the airflows over both the acid and the base solutions were increased from 1 to 5 cc/s. As shown in these figures the aerosol peak is shifted toward smaller sizes when the residence times of the airflows over their respective solutions is decreased. The reduction of the surface area of the acid bath also decreases the mean particle size. An aerosol of larger size particles can be produced by the redirecting the airflow that has passed over the base solution, over the acid, producing size distributions as shown in Fig. A4.

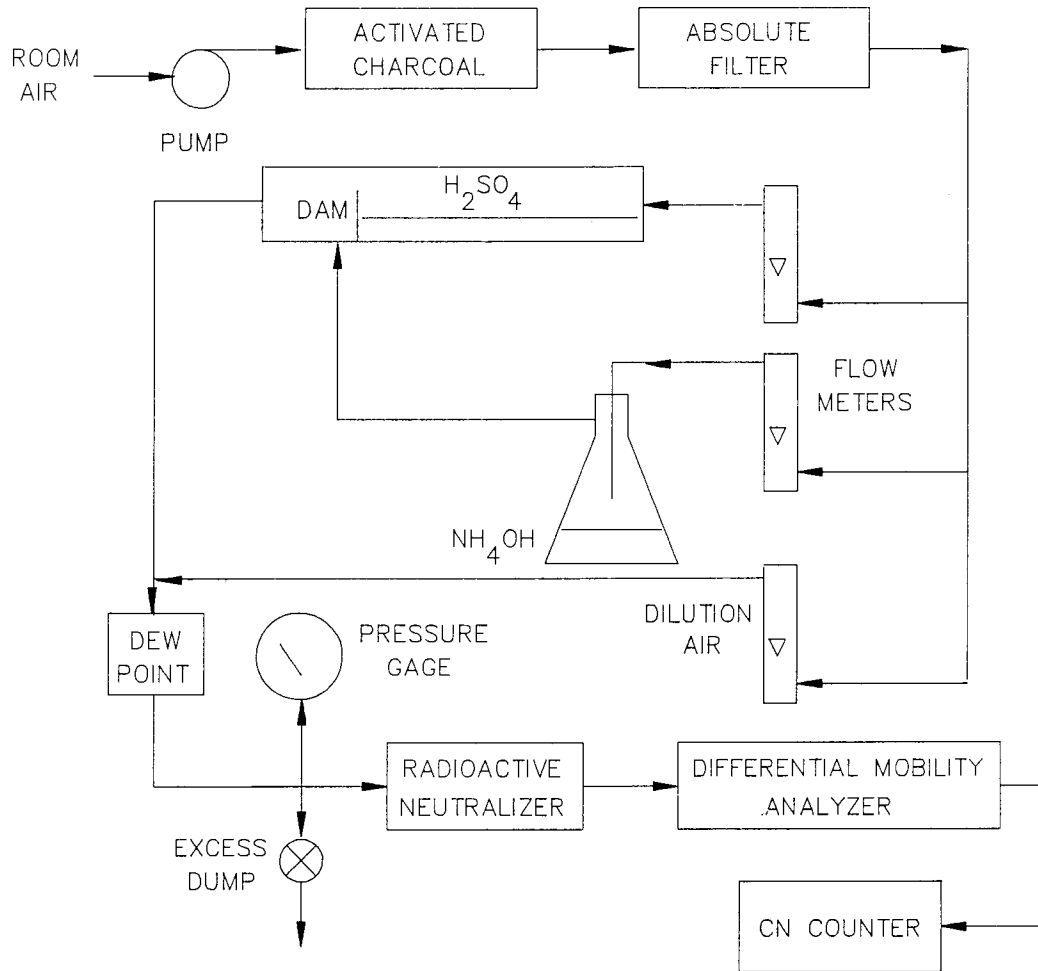


Fig. A1 — Aerosol generation and measurement apparatus

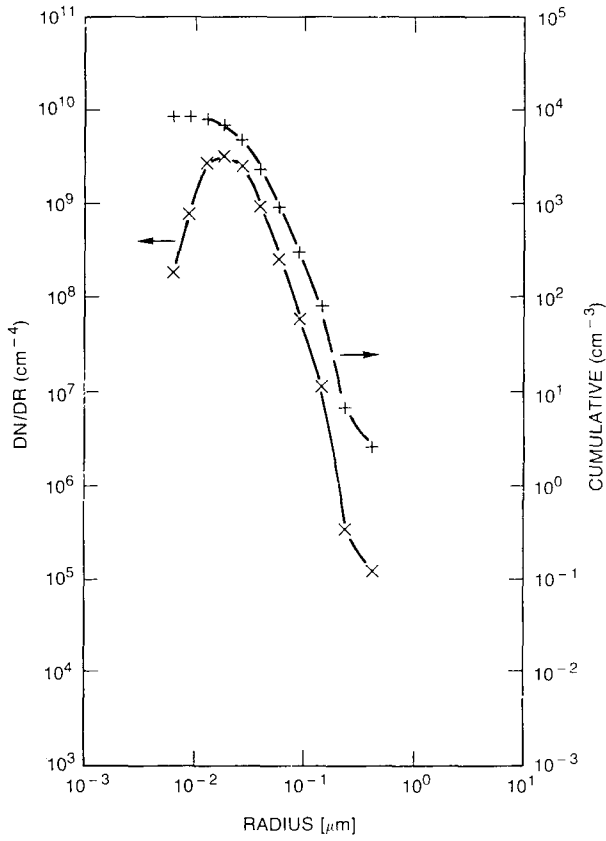


Fig. A2 — Typical size distribution for 1 cc/s flows over acid and base solutions

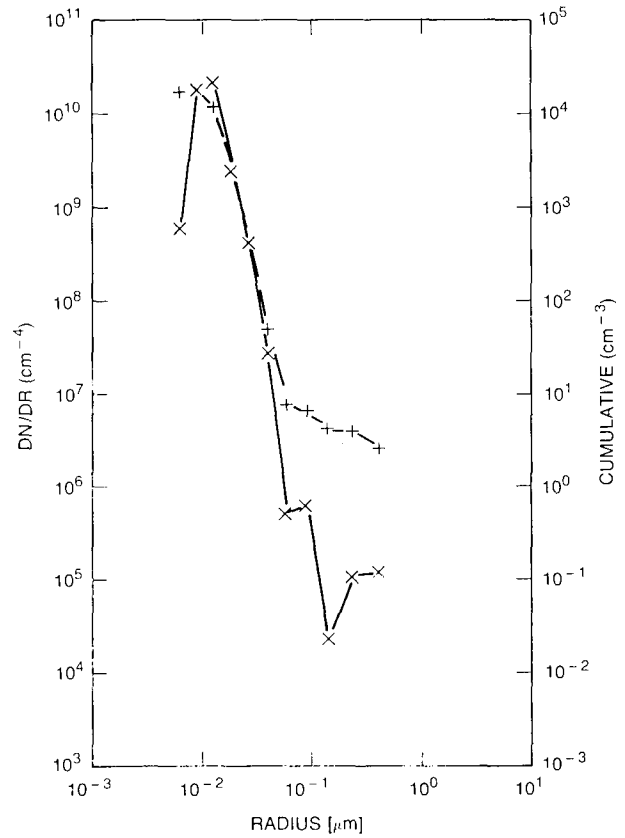


Fig. A3 — Typical size distribution for 5 cc/s flows over acid and base solutions

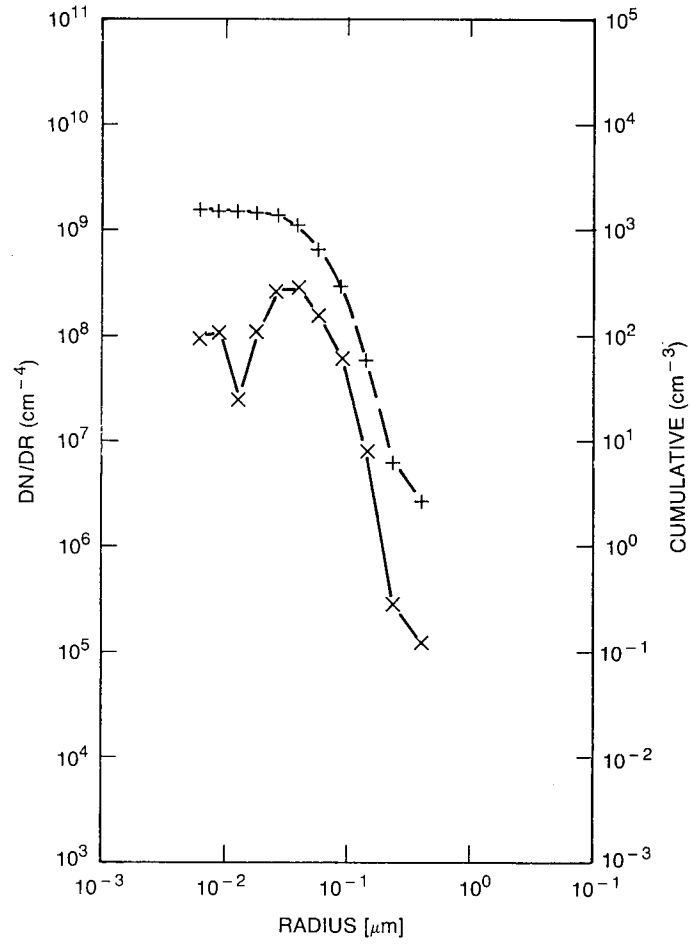


Fig. A4 — Typical size distribution for 1 cc/s flows over the base solution and acid solution (in series)

Appendix B

MEASUREMENTS OF ION CURRENT VS COLLECTOR VOLTAGE

Figures B1 through B4 are I-V curves obtained from the experimental arrangement depicted in Fig. 10, where the radioactive sources consisted of a 1.0 cm diameter, 5.3 μCi Am-241 foil. Five grounded vertical shield wires were placed just upwind of the plate in an effort to reduce the upwind penetration of the field from the plate. Figure B1 shows that when the distance between the foil and collector was 2 cm, the linear (conduction) region of the I-V curve extends from about -2 to $+2$ volts, and the curve flattens as the majority of the ions are collected. The slope of the curve does not go to zero because increased voltage reduces the ion loss by recombination; this also applies to Figs. B2 and B3 for which the source to collector distances were 6.0 and 30 cm respectively. The further the ion collector is from the source, the easier it is obtain current saturation above 2 V because the rate of recombination in the ion collector region is reduced. The numbers near the I-V curves give the slope of the linear portion of the curve in units of Amp Volt^{-1} .

The relative mobilities of the ions can be estimated from the the slopes of the conductive region and the total ion concentration by the use of the following relation:

$$\frac{k_-}{k_+} = \frac{\lambda_- n_+}{\lambda_+ n_-} \quad (\text{b1})$$

where

- k are the ion mobilities,
- λ are the slopes (polar electrical conductivities), and
- n are the ion concentration.

Evaluation of this relation from Fig. B3 ($d = 30$ cm) resulted in a ratio of negative to positive ion mobilities of approximately 1.4. This is significantly greater than the ratio of ion mobilities we used in our aerosol charging theory (Hoppel and Frick, 1986), which are applicable for atmospheric ions. The same theory was used in Section 2 of this report; however it was revised to accommodate the greater difference in ion mobilities. Our calculations of ion deposition in a channel, given in Section 4, used mobilities that gave a ratio of 1.4.

Figure B4 illustrates the large ratio of positive to negative ions that can be obtained with a diffusion cell. For this case the radioactive source was located 12 cm from the shield wires, and the 6 cm immediately in front of the shield wires was occupied by a "diffusion cell" (a set of five parallel plates, each $4.0 \times 6.0 \times 0.05$ cm, discussed in Section 3.2).

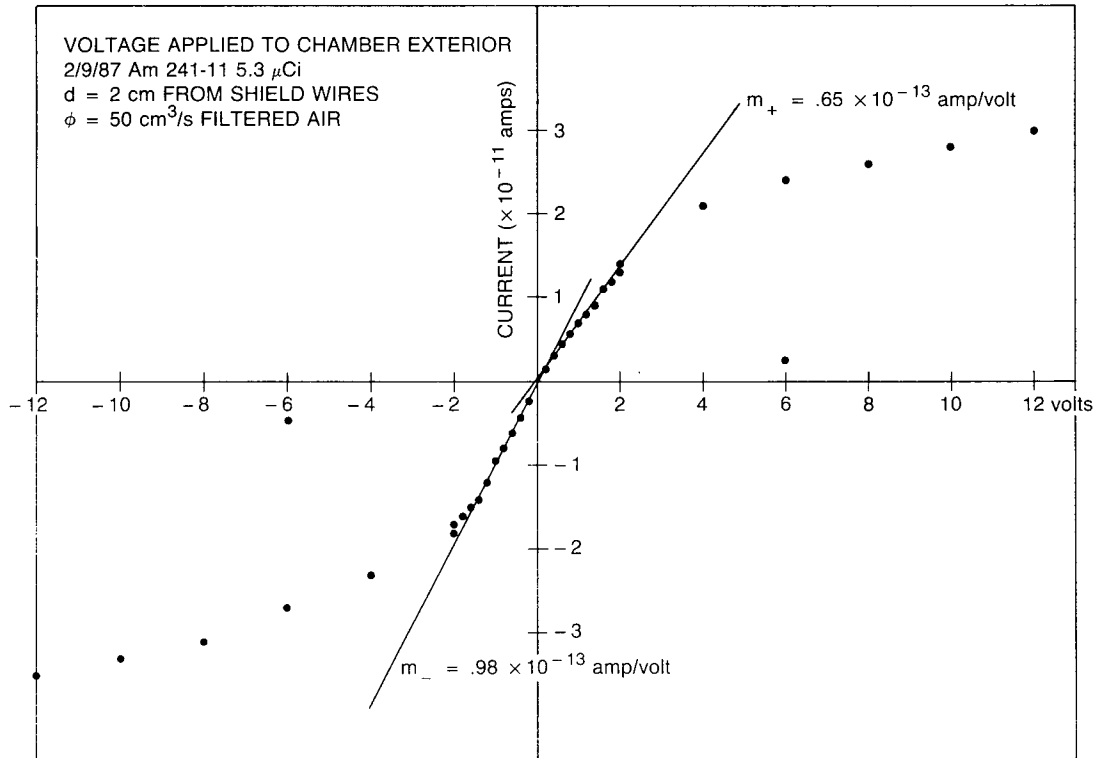


Fig. B1 — I-V curve taken 2 cm from a 5.3 μ Ci Am-241 source

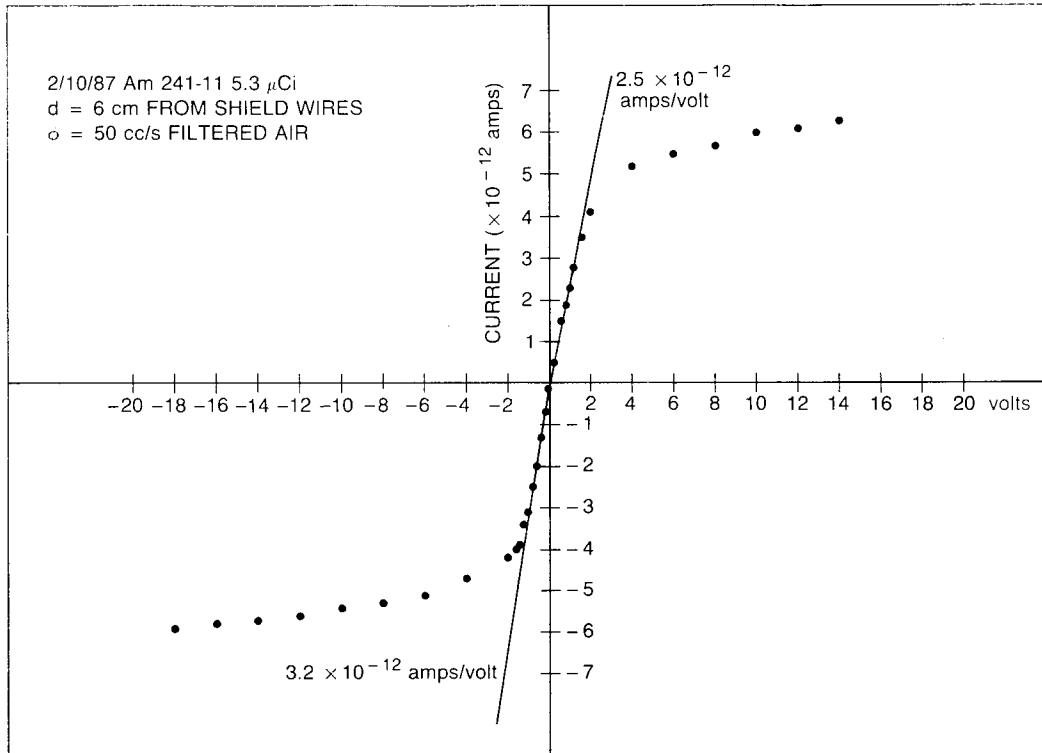


Fig. B2 — I-V curve taken 6 cm from a 5.3 μ Ci Am-241 source

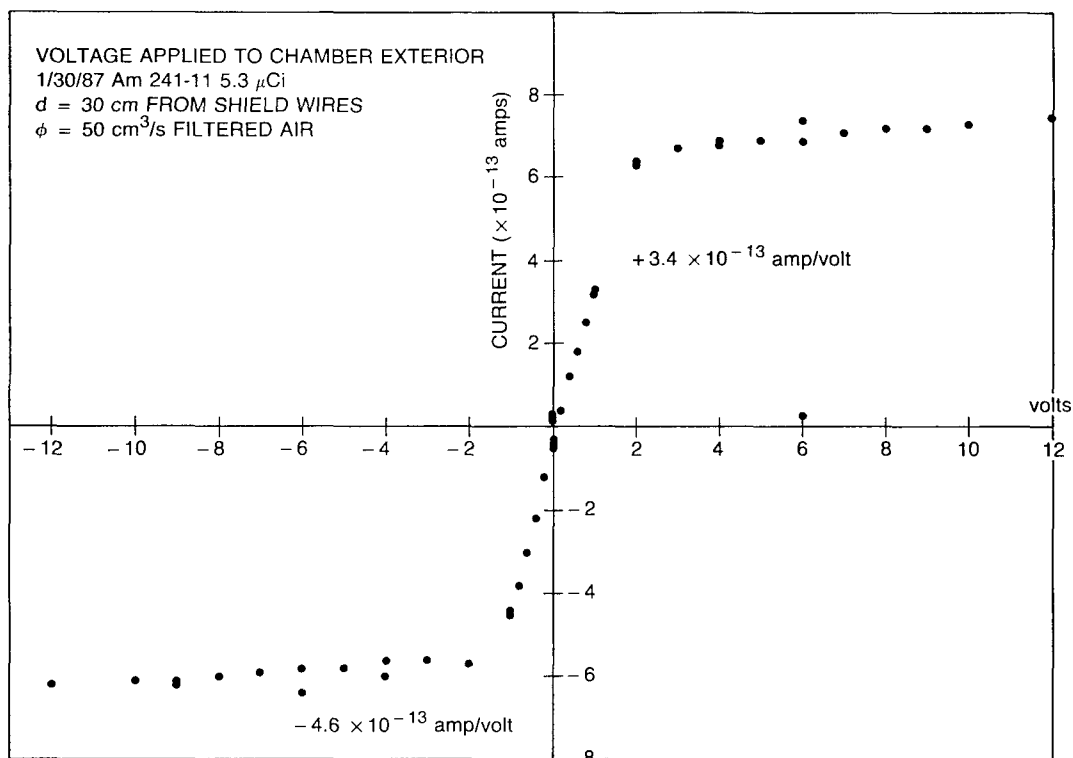


Fig. B3 — I-V curve taken 30 cm from a 5.3 μ Ci Am-241 source

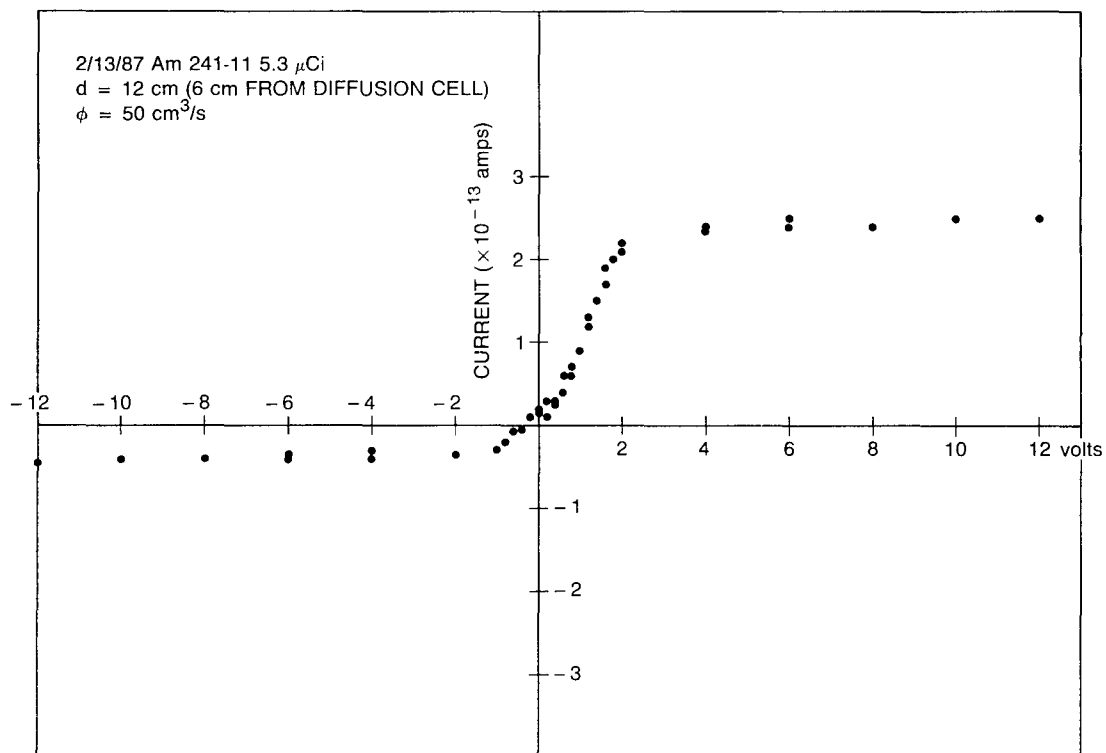


Fig. B4 — I-V curve taken 12 cm from 5.3 μ Ci Am-241 source with an intermediate 6-cm diffusion cell located 6 cm from the source

Appendix C

TIME-DEPENDENT CHARGING CALCULATIONS

We have modeled the time-dependent charging of a monodisperse aerosol by applying a Runge-Kutta method to the combined set of Eqs. (5) to (11). Particles of radius $0.01 \mu\text{m}$ were used in all but one of the following figures because the $0.01\text{-}\mu\text{m}$ particle is within the size range of our interests and lacks the multiple charges that tend to clutter the figure. The concentration of $10,000 \text{ cm}^{-3}$ was chosen as a standard aerosol concentration for comparisons between the figures, thus the results presented here would not apply to concentrations much greater. The bipolar ion production rate of $100,000 \text{ ion pairs cm}^{-3}$ was selected as representative of an instance for which the recombination loss of ions may not necessarily be the predominant loss mechanism. Although wall losses are not included in the aerosol charging calculations, we are considering regimes for which ion losses to walls would appreciably alter the balance of ions. (The effect of walls on the ratio of the ion concentrations was simulated by using different initial ion concentrations, as shown in Fig. 8.)

In Figs. C1 to C4, concentrations of positive (negative) ions are identified by $n_+(n_-)$, the uncharged particles by Os, and the charged particles by the appropriate sign followed by the number of charges.

Figure C1 shows the charging of $0.01\text{-}\mu\text{m}$ particles for an ionization rate of $10^6 \text{ ion pairs/cm}^3/\text{s}$. The relaxation time is reduced to $\sim 3 \text{ s}$ compared to 10 s for Fig. 6 ($10^5 \text{ ion pairs/cm}^3/\text{s}$).

Figure C2 shows that if there were preexisting 5×10^5 concentrations of bipolar ions, the relaxation time is only reduced to about 9 s .

In Fig. C3 the entire population of 10^5 particles has been given a negative single charge, and the relaxation time is about 15 s ; note the equilibrium values for positive and negative particles. Figure C4 shows that if an initial ion imbalance is introduced so as to eliminate the net space charge, the charge equilibrium values will be the same as those in previous figures. This difference in equilibrium is due to the charge conservation built into the governing equations and results in the majority of the space charge being accommodated by an imbalance in the equilibrium ion concentrations, with the remainder carried on the particles.

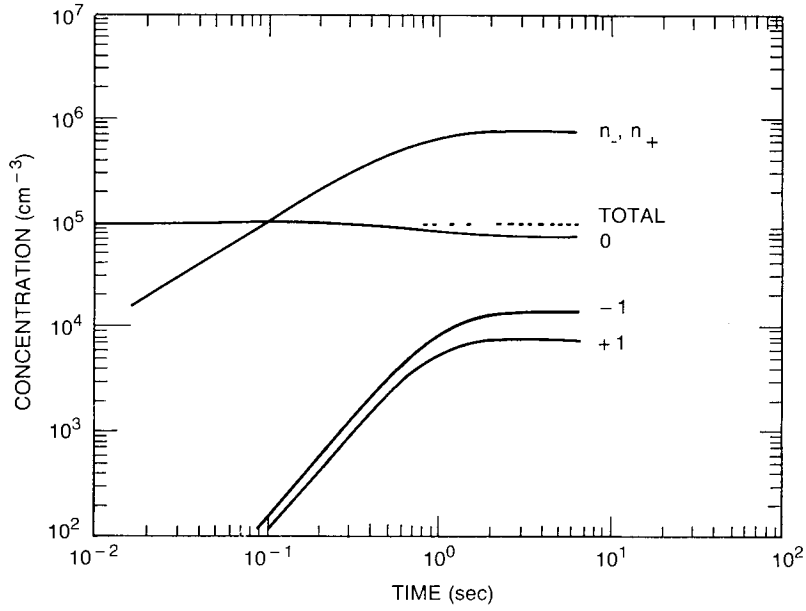


Fig. C1 — Charging of $0.01 \mu\text{m}$ radius particles with an ion source rate of $10^6 \text{ cm}^{-3} \text{ s}^{-1}$ and no initial ion concentrations

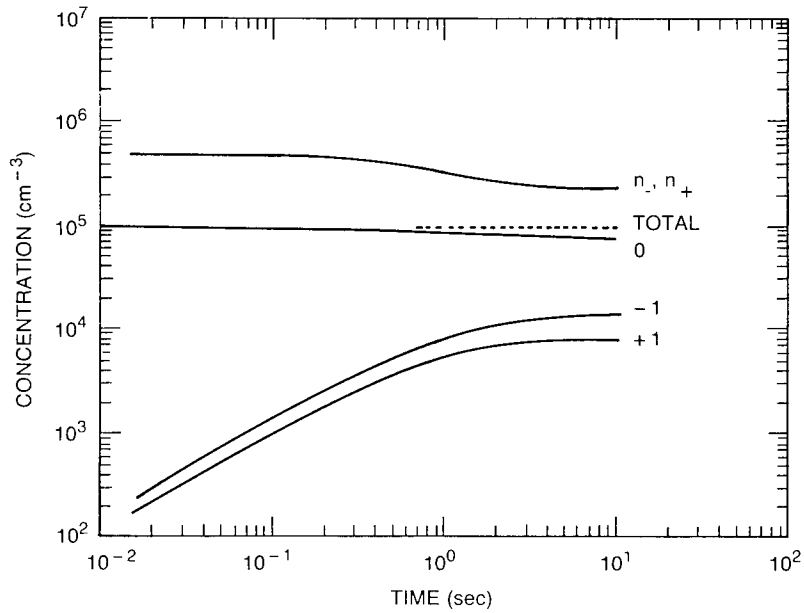


Fig. C2 — Charging of $0.01 \mu\text{m}$ radius particles with an ion source rate of $10^5 \text{ cm}^{-3} \text{ s}^{-1}$ and initial ion concentration of $5.0 \times 10^5 \text{ cm}^{-3}$ for both signs

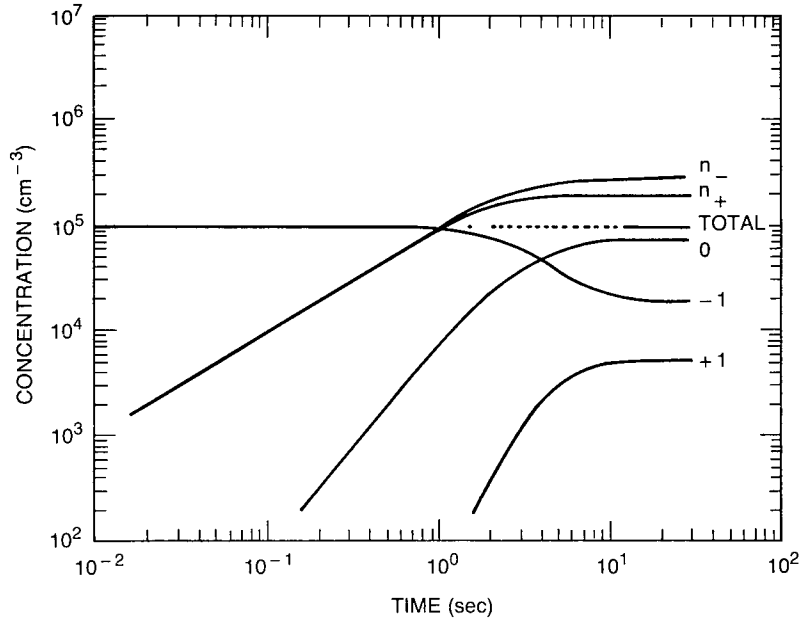


Fig. C3 — Charging of $0.01 \mu\text{m}$ radius particles with an ion source rate of $10^5 \text{ cm}^{-3} \text{ s}^{-1}$, no initial ion concentrations, and all particles initially carry a single negative charge.

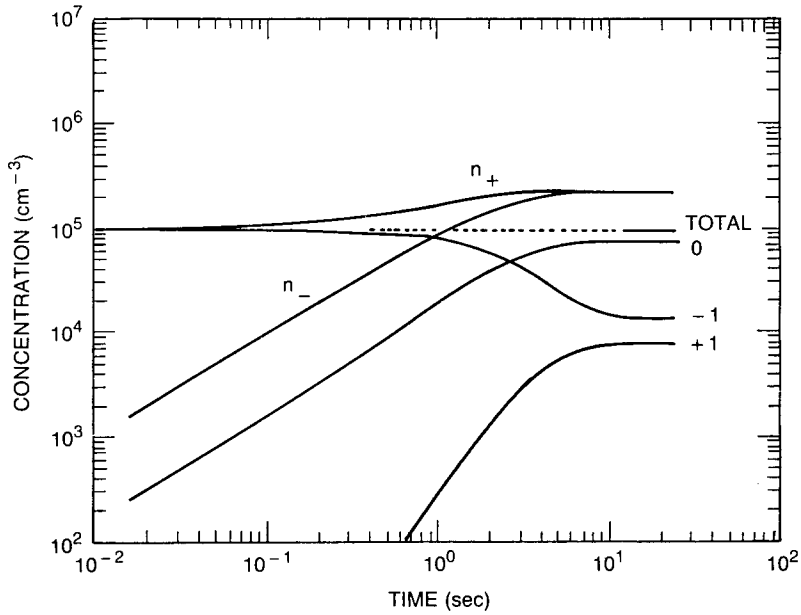


Fig. C4 — Charging of $0.01 \mu\text{m}$ radius particles with an ion source rate of $10^5 \text{ cm}^{-3} \text{ s}^{-1}$, an initial positive ion concentration of 10^5 cm^{-3} , and all particles initially carry a single negative charge

Appendix D

ION AEROSOL ATTACHMENT COEFFICIENT CALCULATION

It is clear from the calculations carried out in this report that the physical properties of the ions are important factors in determining the ion-aerosol attachment coefficients. Particularly important is the ratio of the positive to negative diffusion coefficient in establishing the ratio of positively to negatively charged particles (Eqs. (9) to (11)). The ion species changes with age as a result of charge exchange between molecules of different ionization potential or electron affinities, and chemical and clustering processes. Ionic mass as a function of age has been measured by a number of investigators, but the ionic chemistry is extremely complex and depends on the concentration and types of trace gases in the air [see for example, Huertas and Fontan (1975); Huertas et al. (1978); Mohnen (1977); and Perkins and Eisele (1984)]. There is currently no consensus on the ionic species that exists in "real" air at atmospheric pressure on the time scales of interest in the neutralizer. Most definitive data have come from mass spectroscopic measurements and at times that correspond to microseconds when converted to atmospheric pressure. Since the molecular collision rate is of the order of 10^{10} s^{-1} , the ion will suffer collisions with trace gases at the ppb level in less than a second. The chemistry of the initial ion probably bears little resemblance to the ions that exist after tens of milliseconds. Measured values of ion mobilities (and recombination coefficients) seem to fall into three classes of measurements: (1) initially formed ions of very short lifetime made in ultrapure air at low pressures, (2) ions with a lifetime of the order of a second in artificially ionized air at about atmospheric pressure, and (3) atmospheric ions that have lifetimes of hundreds of seconds and exist in concentrations of 100 to 1000 cm^{-3} . Atmospheric ions have reduced mobilities of about 1.15 and 1.25 $\text{cm}^2 \text{ V}^{-1} \text{ s}^{-1}$ for positive and negative ions respectively [Mohnen, (1977)] and a recombination coefficient of $1.4 \times 10^{-6} \text{ cm}^3 \text{ s}^{-1}$ [Nolan, (1943)].

There have been many measurements of ion mobilities in the laboratory, with ions generated by various artificial ionization sources dating back to the early 1900s when ions were first discovered. In these experiments the ion concentrations are much greater than in the atmosphere, and therefore the ion lifetime is much less. For instance, the recombination lifetime of ions at a concentration of 10^6 is less than 1 s. A table of mobility values measured by different authors in air of various degrees of purity and various ionization sources is given by Mohnen (1977). The average mobilities of these ten measurements are 1.33 and 1.84 $\text{cm}^2 \text{ V}^{-1} \text{ s}^{-1}$ at STP with a negative to positive mobility ratio of about 1.4. The conditions under which these measurements were made are more like those that must exist in ionizers than atmospheric conditions.

In our earlier work [Hoppel, (1985); Hoppel and Frick (1986)]; we were interested primarily in atmospheric ions and we used positive and negative mobility values of 1.2 and 1.35 $\text{cm}^2 \text{ V}^{-1} \text{ s}^{-1}$. This gives a negative to positive mobility ratio of only 1.12. While these values are probably the best available for aged tropospheric ions, they are clearly not the best values for conditions which exist in ionizers. We have therefore recalculated all the ion-aerosol coefficients using positive and negative mobility values of 1.3 and 1.8, respectively.

In addition to the mobilities, the ionic masses are also required for the calculation of the ionic mean-free-paths. The mean free path is directly proportional to the mobility and inversely proportional to the factor

$$\left(1 + \frac{M_{\text{air}}}{M_{\text{ion}}} \right)^{1/2}$$

which is a much weaker dependence since the ionic mass M_{ion} is much greater than the mass of the air molecule M_{air} (28.8 AMU). There is not a unique relationship between mobility and ionic mass; but empirical plots of mass vs mobility [Cabane et al. (1976), Huertas et al. (1974), and Meyerott et al. (1980)] indicate that for the mobilities used here, ionic masses of 200 AMU and 100 AMU for positive and negative ions are very reasonable values.

The ion-aerosol attachment coefficients have been recalculated for positive and negative ions with the properties cited above and are given in Tables D1 and D2 and plotted in Fig. D1. The procedure used is that presented in Hoppel and Frick (1986) with one modification. In the case of non-symmetric ion properties, the electrostatic energy gained by the two ions during an encounter is different, and the energy loss required for trapping is different for the two ions. Instead of adjusting the ion-aerosol trapping distance using the functional relationship given in our earlier paper, we here adjusted the energy required to ensure trapping. The energy loss required to ensure trapping, calculated for ion-ion recombination was then partitioned between the two ions (for the ion-aerosol encounter) in a manner which accounts for the fact that the negative (lighter) ion acquires more electrostatic energy than the positive ion and the fact that the negative ion loses more energy during a collision with a neutral molecule because it is lighter. The ion-aerosol trapping distances are then calculated from Eq. (34) of Hoppel and Frick (1986) separately by using different energies for positive and negative ions. Both the old and new method give the same result when the particles are small ($r < 0.02 \mu\text{m}$), but when the polar ions have large differences in mobilities as is the case here, then the old method leads to errors at intermediate sizes.

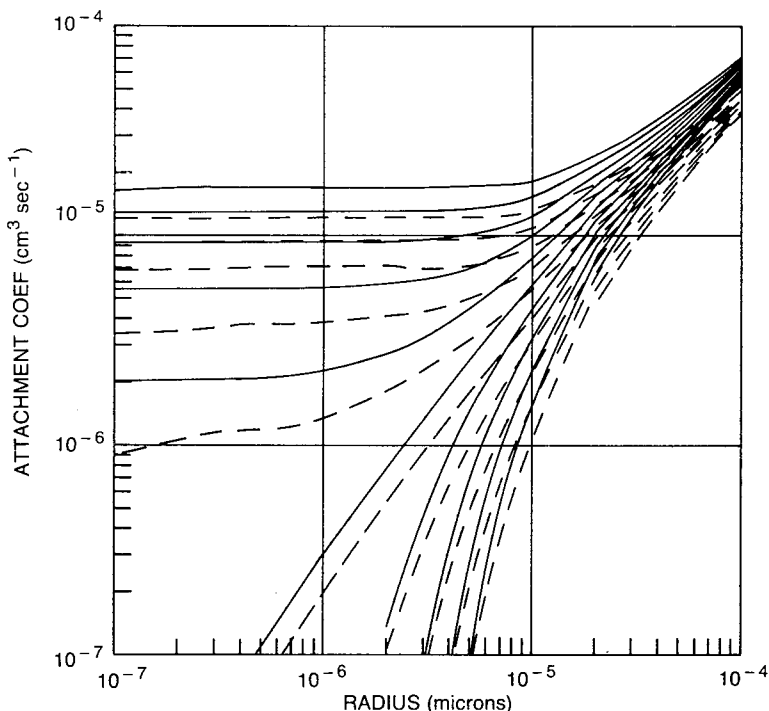


Fig. D1 — Attachment coefficients vs radius, as given in Tables D1 and D2

Table D1 — Attachment Coefficients For 200 AMU Ions ($\text{cm}^3 \text{s}^{-1}$) (multiply by 10^6)

Radius (μm)	Discharging					Charging				
	Number of Charges					Number of Charges				
	5	4	3	2	1	0	1	2	3	4
0.001	12.12	9.30	6.81	3.39	.899	0.006	0.000	0.000	0.000	0.000
0.002	12.12	9.31	6.86	3.49	1.06	0.017	0.000	0.000	0.000	0.000
0.003	12.13	9.34	6.92	3.61	1.17	0.031	0.000	0.000	0.000	0.000
0.004	12.15	9.37	7.01	3.76	1.17	0.049	0.000	0.000	0.000	0.000
0.005	12.18	9.43	7.11	3.76	1.19	0.069	0.000	0.000	0.000	0.000
0.006	12.21	9.46	7.11	3.76	1.20	0.091	0.000	0.000	0.000	0.000
0.007	12.21	9.46	7.11	3.77	1.23	0.115	0.000	0.000	0.000	0.000
0.008	12.21	9.46	7.11	3.77	1.26	0.141	0.000	0.000	0.000	0.000
0.009	12.21	9.46	7.12	3.84	1.30	0.168	0.000	0.000	0.000	0.000
0.010	12.21	9.46	7.12	3.85	1.34	0.197	0.000	0.000	0.000	0.000
0.020	12.22	9.48	7.19	4.11	1.83	0.539	0.104	0.000	0.000	0.000
0.030	12.25	9.56	6.88	4.31	2.29	0.941	0.342	0.079	0.000	0.000
0.040	12.31	9.61	6.99	4.65	2.75	1.37	0.655	0.256	0.077	0.009
0.050	12.29	9.68	7.21	5.01	3.21	1.82	1.02	0.500	0.221	0.083
0.060	12.30	9.83	7.49	5.41	3.68	2.28	1.41	0.797	0.422	0.206
0.070	12.46	10.29	7.85	5.83	4.15	2.74	1.83	1.13	0.670	0.377
0.080	12.63	10.32	8.21	6.26	4.63	3.21	2.26	1.50	0.958	0.591
0.090	12.86	10.62	8.59	6.70	5.10	3.68	2.70	1.88	1.28	0.843
0.100	13.45	10.95	8.95	7.15	5.57	4.14	3.15	2.29	1.62	1.12
0.200	16.75	14.97	13.30	11.75	10.30	8.85	7.78	6.70	5.73	4.87
0.300	21.01	19.39	17.85	16.38	14.99	13.52	12.42	11.27	10.20	9.20
0.400	25.49	23.95	22.47	21.05	19.63	18.18	17.09	15.91	14.78	13.72
0.500	29.99	28.50	27.06	25.66	24.24	22.77	21.69	20.49	19.34	18.23
0.600	34.52	33.07	31.65	30.27	28.84	27.42	26.29	25.08	23.91	22.77
0.700	39.10	37.67	36.28	34.91	33.47	31.96	30.93	29.71	28.52	27.36
0.800	43.68	42.27	40.89	39.53	38.08	36.55	35.54	34.31	33.11	31.94
0.900	48.24	46.84	45.47	43.97	42.66	41.21	40.12	38.88	37.68	36.50
1.000	52.78	51.40	50.03	48.52	47.21	45.75	44.67	43.43	42.22	41.03
2.000	97.97	96.64	95.33	94.03	92.74	91.16	90.20	88.95	87.71	86.48
3.000	143.1	141.8	140.5	139.2	137.9	136.6	135.3	134.1	132.8	131.6

Table D2 — Attachment Coefficients For 100 AMU Ions ($\text{cm}^3 \text{s}^{-1}$) (multiply by 10^6)

Radius (μm)	Discharging					Charging				
	Number of Charges					Number of Charges				
	5	4	3	2	1	0	1	2	3	4
0.001	16.40	12.82	9.26	5.53	2.01	0.009	0.000	0.000	0.000	0.000
0.002	16.96	12.95	9.26	5.54	2.03	0.026	0.000	0.000	0.000	0.000
0.003	16.96	12.95	9.27	5.55	2.05	0.049	0.000	0.000	0.000	0.000
0.004	16.96	12.95	9.27	5.55	2.07	0.077	0.000	0.000	0.000	0.000
0.005	16.96	12.96	9.27	5.56	2.10	0.108	0.000	0.000	0.000	0.000
0.006	16.96	12.96	9.28	5.57	2.13	0.142	0.000	0.000	0.000	0.000
0.007	16.96	12.96	9.28	5.59	2.16	0.180	0.000	0.000	0.000	0.000
0.008	16.96	12.96	9.29	5.60	2.19	0.220	0.000	0.000	0.000	0.000
0.009	16.97	12.97	9.29	5.61	2.23	0.263	0.000	0.000	0.000	0.000
0.010	16.97	12.97	9.30	5.63	2.27	0.307	0.000	0.000	0.000	0.000
0.020	17.01	13.04	9.44	5.91	2.74	0.777	0.137	0.000	0.000	0.000
0.030	17.15	13.20	9.65	6.18	3.26	1.36	0.491	0.087	0.000	0.000
0.040	17.20	13.29	9.83	6.56	3.90	1.98	0.954	0.356	0.080	0.000
0.050	17.29	13.45	10.12	7.06	4.58	2.62	1.48	0.722	0.299	0.088
0.060	17.44	13.69	10.52	7.63	5.25	3.28	2.06	1.16	0.600	0.276
0.070	17.66	14.02	11.00	8.24	5.93	3.94	2.66	1.65	0.969	0.535
0.080	17.59	14.42	11.52	8.86	6.60	4.60	3.28	2.18	1.39	0.855
0.090	17.93	14.95	12.04	9.49	7.27	5.26	3.91	2.74	1.86	1.22
0.100	18.33	15.43	12.61	10.12	7.94	5.93	4.55	3.32	2.36	1.64
0.200	23.50	21.05	18.74	16.59	14.58	12.56	11.07	9.56	8.21	7.00
0.300	29.46	27.22	25.08	23.05	21.09	19.09	17.57	15.97	14.47	13.08
0.400	35.64	33.52	31.46	29.49	27.62	25.52	24.09	22.45	20.89	19.40
0.500	41.96	39.90	37.90	35.89	34.03	31.98	30.50	28.84	27.23	25.70
0.600	48.26	46.24	44.28	42.28	40.43	38.35	36.91	35.23	33.60	32.02
0.700	54.63	52.65	50.59	48.72	46.89	44.76	43.36	41.67	40.02	38.42
0.800	60.85	58.90	56.83	54.96	53.14	51.13	49.62	47.91	46.25	44.63
0.900	67.17	65.23	63.15	61.30	59.48	57.46	55.96	54.25	52.58	50.94
1.000	73.62	71.51	69.64	67.80	65.99	63.75	62.46	60.75	59.07	57.42
2.000	136.1	134.2	132.4	130.6	128.8	127.0	125.3	123.6	121.9	120.2
3.000	198.5	196.7	194.9	193.1	191.3	189.5	187.8	186.1	184.3	182.6

